

Study of gaseous detectors for high energy physics experiments

A thesis Submitted
in Partial Fulfilment of the Requirements
for the Degree of

MASTER OF SCIENCE

by

Sumanya Sekhar Sahoo



School of Physical Sciences
National Institute of Science Education and Research
Bhubaneswar

Abstract

Gas filled detectors are one of the oldest and most widely used radiation detectors and based on the effects produced when a charged particle passes through a gas. Many ionization mechanism arise in gases and over the years these have been studied and exploited in the detector. In this particular work we have studied a few aspects of these different phenomena. We have described here the principles of operation of the gas ionization chamber focussing on the most relevant mechanisms involved in the detection process. This knowledge is necessary to understand, simulate and optimize the performance of the proposed or any existing detection system. The simulation procedure is now-a-days widely utilize in designing such detectors. Starting with the basic principle of operation of gas detectors, we first discuss the different regions of operation of gas detectors. Following which, the production of primary and secondary electrons, transport of charged particle in gases, the electron multiplication process, the required characteristics of the gas mixture have been described. Then we illustrate the basic features of some gas detectors. We also give a brief idea about the simulation and present some calculation utilizing various computer programmes.

ACKNOWLEDGEMENTS

I thank to Dr. Bedangadas Mohanty for his constant support, Dr. Purba Bhat-tacharya for her detailed guidance and Dr. Saikat Biswas for the clarification of my doubts when ever needed.

Contents

1	Introduction	1
2	Basic Principles of interaction of radiation with matter	6
2.1	Interaction of radiation and matter	6
2.1.1	Interaction of charged particles in a gas	7
2.1.2	Interaction of neutral particles in a gas	9
2.2	Ionisation Detectors	10
2.2.1	Gaseous ionisation Detectors	11
2.2.2	Choice of Gas	14
2.3	Energy loss	16
2.4	Different types of ionisation mechanism	18
3	Energy loss of Charged Particles	20
3.1	Bethe-Bloch formula	20
3.2	Photoabsorption ionization model	25
3.2.1	Cross Section for Ionizing Collisions	25
3.2.2	Energy Loss Simulation	28
4	Transport of charged particle in Gases	29
4.1	Drift of Charged Particle	31
4.2	Microscopic Picture	33
4.2.1	Drift of Electrons	33
4.3	Drift of Ions	35
4.4	Inclusion of Magnetic Field	36
4.5	Diffusion	37
4.6	Electric Anisotropy	42
4.7	Magnetic Anisotropy	43
4.8	Amplification	44
4.8.1	Electron multiplication of the gas	44
4.8.2	The first Townsend coefficient	47
4.8.3	The Second Townsend Coefficient	48
4.9	Electron loss	49
4.9.1	Recombination	49
4.9.2	Electron Attachment	50
5	Measurement of Ionization	52
5.1	Signals Induced on Grounded Electrodes, Ramos Theorem	52
5.2	Induced Signals in a Drift Tube	54
6	Simulation of Gaseous detectors	58
6.1	Simulation tools	59
6.1.1	Garfield	60
6.1.2	MAGBOLTZ	61
6.1.3	Calculation of the electric field	67
6.1.4	Accuracy check of neBEM	71

7	Results and Discussion	74
7.1	Multi Wire Proportional Chamber	74
7.2	Gas Electron Multiplier	76
7.2.1	Principle of operation	77
7.2.2	Results	83
7.2.3	Conclusion	89
8	Summary and Conclusions	90
	References	91

List of Figures

1.1	Various types of detection techniques	2
2.1	Schematic setup for a gaseous ionisation detector.	12
2.2	I-V characteristics of Gas detectors.	13
2.3	Ionisation mechanisms considering Bohr's model of an atom.	19
3.1	Incoming fast particle of charge ze scattered by an atomic electron almost at rest: for small energy transfer, the particle trajectory is not deflected	21
3.2	An incoming fast particle of charge ze interacts with electrons at impact parameter between b and $b + db$	22
4.1	Mobility variation inside an electron cloud travelling in the z direction.	43
4.2	Process of recombination and Ionisation.	50
5.1	Cylindrical proportional tube with outer radius b at voltage V_0 and inner (wire) of radius a at voltage zero.	55
5.2	Current signal according to Eq-5.19 (full line, left-hand scale) for $t_0 = 1.25ns$, $b/a = 500$, and $q = 10^6 * e$. Time integral of this pulse (Induced charge) as a percentage of the total (broken line, right-hand scale)	57
6.1	An overview of the different methods on quest of truth is explained through a flow chart	59
6.2	Variation of drift velocity of electron in different gas mixtures.	62
6.3	Variation of Townsend coefficient of electron in different gas mixtures.	63
6.4	Variation of attachment coefficient of electron in different gas mixtures.	63
6.5	Variation of longitudinal diffusion coefficient of electron in different gas mixtures.	64
6.6	Variation of Transverse diffusion coefficient of electron in different gas mixtures.	64
6.7	Variation of longitudinal diffusion coefficient of electron in $Ne-CO_2-N_2$ (90-10-5) with magnetic field.	65
6.9	Variation of transverse diffusion coefficient of electron in $Ne-CO_2-N_2$ (90-10-5) with magnetic field (Perpendicular to electric field).	66
6.8	Variation of transverse diffusion coefficient of electron in $Ne-CO_2-N_2$ (90-10-5) with magnetic field (parallel to electric field).	66
7.1	Schematic diagram of a MWPC read out and use of gating grid.	75
7.2	Volatage and Electric field configuration of MWPC.	75
7.3	Simulating an Avalanche in MWPC.	76
7.4	Image of the GEM foil taken with an electron microscope.	78
7.5	Schematic diagram of a GEM detector's readout.	79
7.6	Basic GEM cell built using Garfield.	81
7.7	Voltage and Electric field along the z -axis passing through hole of a GEM.	81
7.8	Electron drift lines in GEM.	82

7.9	A simulated avalanche, drift and the diffusion of secondary electrons (blue) and ions (yellow).	83
7.10	Variation of electron transmission and efficiencies as a function of drift field.	85
7.11	Variation of electron transmission and efficiencies a function of induction field.	85
7.12	Variation of electron transmission and efficiencies a function of GEM voltage (For different pitch).	86
7.13	Variation of IBF a function of drift and induction field.	87
7.14	Variation of IBF as a function of GEM voltage (For different pitch).	88
7.15	Variation of Gain as a function of GEM Volatge.	89

List of Tables

6.1	Comparison of theoretical calculation and neBEM field values.	72
-----	---	----

Chapter 1

Introduction

The history of the nuclear and elementary particle physics has seen the development of many different types of detectors to detect and quantitatively measure various types of radiations. In order to detect a radiation we convert its energy to a known measurable form. For example when a charged particle or radiation passes through gas it loses its energy which can be collected in a electrical signal by applying electric field.

Particles and radiation can be detected only through their interactions with matter. There are specific interactions for charged particles which are different from those of neutral particles, e.g. of photons. One can say that every interaction process can be used as a basis for a detector concept. The variety of these processes is quite rich and, as a consequence, a large number of detection devices for particles and radiation exist.(Fig-1.1) In addition, for one and the same particle, different interaction processes at different energies may be relevant. Calculations for gas-based detectors have 3 main components: ionisation, field calculation and charged particle transport. A Time Projection Chamber (TPC), is an advanced particle detector for detecting charged particles. It is capable of 3D tracking. The momentum measurements and particle identification can be achieved through energy loss measurements, if it is placed in a solenoidal magnetic field. A TPC usually consists of a gas filled cylindrical drift volume. An uniform electric field is applied over the drift volume, usually with the anodes at the two ends of the chamber and the cathode in the middle, dividing the chamber in two halves. The homogeneity of the electric field is provided by a

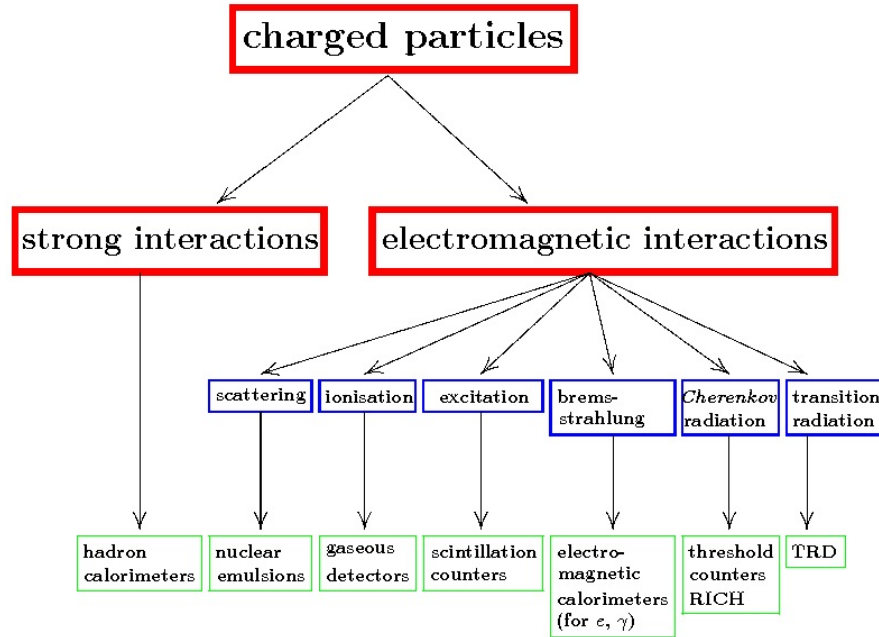
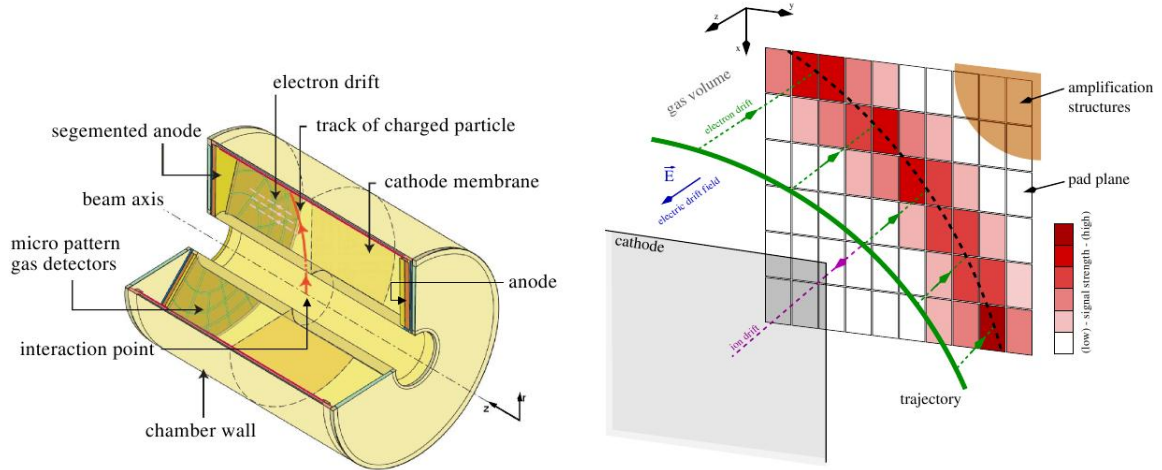


Figure 1.1: Various types of detection techniques

field cage that consists of equidistant ring of electrodes placed along the TPC. The ring-electrodes are powered with constant potential differences between the cathode and anode plane. When a charged particle crosses the gas, it produces ionization along its trajectory. Driven by the electric field, the electrons separate from the gas ions and drift towards the read-out plane. This means that the electric field shifts an image of the trajectory to the read-out - in the best case without any deformations. Directly in front of the read-out plane, the electrons are multiplied in the amplification structures. The amplification is necessary because an initial particle creates only about 100 electron-ion pairs per centimeter which are too small to produce sufficiently strong signals on the read-out plane. Finally, a signal density distribution is measured which represents a projection of the trajectory onto the read-out plane. X and Y coordinates are obtained from the detection plane and the Z coordinate from the drift time. A computer algorithm then reconstructs the trajectory from the signal

distributions on the pads and corresponding drift times. A schematic diagram of the TPC and its operating principle are shown in Figure below.



The conventional read-out system in the TPCs are the MWPCs.. But the ion feedback problem restricts the use of the MWPC in high rate experiments. The ions created in the amplification process, drift back into the TPC volume, create local perturbations in the electric field and, thus, affect the drift behavior of the electrons from a later track. This can be solved by using an additional plane of gating wires which has to be activated through some trigger mechanism. Compared to a typical MWPC , a typical triple GEM detector represents roughly 3 times the material budget. In many other aspects GEM detectors exceed the performance of wire chambers. Most notably, GEM detectors feature probably the highest rate capability of any gaseous detector. GEM s are also much more resilient to aging, particularly in Ar/CO_2 gas mixtures. What makes GEM detectors attractive from a practical point of view are a relatively low cost of production and operation, and the fact that they are essentially maintenance free.

There are some intrinsic differences between these two gas detectors. In a GEM detector, the GEM foil screens the movement of ions (above the GEM) from the

readout elements (below), thereby eliminating the characteristic ion tails in the signals of MWPCs. In wire chambers, ions generated in the avalanche remain in the gas for tens or hundreds of microseconds, reducing the field strength around the anode wires (and therefore the gas gain). The ions generated in a GEM avalanche leave the hole within ~ 100 ns, which explains the orders of magnitude higher rate capability of GEMs.

Wire chambers also suffer from aging. The mechanisms and failure modes depend on the radiation environment and gas mixture. The avalanche plasma tends to introduce free radicals in the gas, and deposit various sorts of chemical compounds on the wire surface. The results are often non-uniformity of gain over the sensitive area and broken wires. GEMs have proven to be much less prone to aging, and their limits of integrated charge still need to be found.[10]

We have described here the principles of operation of the gas ionization chamber focusing on the most relevant mechanisms involved in the detection process. This knowledge is necessary to understand, simulate and optimize the performance of the proposed or any existing detection system. The simulation procedure is now-a-days widely utilized in designing such detectors. Starting with the basic principle of operation of gas detectors, we first discuss the different regions of operation of gas detectors. Following which, the production of primary and secondary electrons, transport of charged particle in gases, the electron multiplication process, the required characteristics of the gas mixture have been described. Then we illustrate the basic features of some gas detectors. As a final point we give a brief idea about the simulation and present some calculation utilizing various computer programmes. The program GARFIELD, written by Rob Veenhof, is the most widely used tool for drift chamber simulation. For calculation of the primary ionization of fast particles in gases, the program HEED, written by Igor Smirnov, is widely used. A very popular program

for calculation of electron transport properties in different gas mixtures is the program MAGBOLTZ, written by Steve Biagi. MAGBOLTZ and HEED are directly interfaced to GARFIELD, which therefore allows a complete simulation of the drift chamber processes, from the passage of the charged particle to the detector output signal.

Chapter 2

Basic Principles of interaction of radiation with matter

A gas ionization chamber consists of a closed volume filled with the adequate gas within an electric field between an anode and cathode plate. When a particle enters into the volume, it interacts with the gas and ionize the atoms of the gas. If the electric field is intense enough, the electrons are highly accelerated and they further ionize the gas. Under these conditions, the number of electrons grows rapidly forming what is known as avalanche. The created electrons and ions drift towards the anode and cathode. The motion of electrons and ions in the gas gives rise to an electric signal on the electrodes which can be detected by an external circuit. For a given gas, the magnitude of the induced signals depend mainly on the field strength and one can distinguishes various modes and regions of operation.

2.1 Interaction of radiation and matter

The effects of a particle traveling through matter depend on its nature and the environment encountered. The electric charge of the particle or its absence determines the type of interaction or behaviour.

A charged particle passing through the electronic clouds of atoms would continuously tear away some of their electrons, a phenomenon called "ionization" . Neutral particles, gamma or neutron do not interact in a progressive manner. They set in motion of charged particles : a gamma would knock on an atomic electron, a neutron a proton or a light nucleus. These secondaries particles will in turn ionize the

atoms. Ionised atoms generally reorganize themselves by emitting photons, among them characteristics X-rays.

2.1.1 Interaction of charged particles in a gas

An electrical charge (just like gravitational mass) gives a particle the ability to act over large distances, allowing it to remove electrons from atoms in the material it passes through. This phenomenon is known as ionization, and the neutral atoms that have lost electrons have become ions. The greater the electrical charge on a particle, the greater its ionizing capability. An alpha or beta particle has an energy some hundreds of thousands of times larger than the few electron-volts needed to ionize most atoms. It would take some 30 eV to remove an electron from a gaseous atom, and far less to remove one from a crystalline structure. The silicon crystals used in certain detectors (and microchips), for instance, only need 3 eV for an electron to be liberated. An alpha particle with an energy of 3 MeV, therefore, can either ionize some 100,000 gaseous atoms or close to a million silicon crystals atoms.

From Bethe-Bloch formula (2.1) it is clear that the energy loss due to ionization is proportional both to the particles mass and to the square of its charge. It also changes dramatically with speed: when the particle is slower, it spends more time in the atom and has a higher chance of interacting with it while it passes through. As a result, ionization becomes particularly intense near the end of the trajectory, when the particles have lost most of their energy. This property is frequently used in therapy; the irradiation of cancerous tumors relies on curving trajectories so that the radioactive particles target the malignant cells. Liberating many electrons uses a great deal of energy, and the particles finally come to a halt. The greater the ionization capability, the shorter the distance these particles can cover. This is especially true

for the alpha particles, where the length of the trajectory depends on their initial energy.

Beta particles have winding tracks that nevertheless cannot surpass a certain maximum length characteristic of the initial energy. From a protection point of view, a layer of armour that is thicker than this maximum length should achieve the required levels of safety. Electrically charged particles lose energy progressively as they travel: by liberating electrons from the atoms that they come across. They gradually slow down and then come to a complete stop. Alpha particles are small nuclei whose energy is not high enough (with a few exceptions) to induce a nuclear reaction. They interact essentially with the medium they pass through because of their electric charge. They are strongly ionizing and easy to stop, but are much more dangerous than beta rays in case of ingestion or inhalation.

Nuclear fission that takes place in nuclear reactors produces also charged nuclei (known as fission products) that inherit most of the liberated energy. This energy will slowly be dissipated through interactions with atoms along a very short trajectory. Heavier than alpha particles, fission products have a proportionally greater electric charge. They are extremely ionizing. Each of them take away an energy some 25 times higher than the 4 MeV given to an alpha particle. This energy is converted into heat, which is at the origin of the electricity produced by nuclear reactors.

Electrons or positrons also interact with the medium through their electric charge, which is far smaller than that of a nucleus. While alpha particles travel in short, straight lines, beta particles (some 8,000 times lighter) have long, unpredictable, chaotic trajectories with numerous abrupt changes of direction.

As a result of their low mass, beta particles are faster than their alpha cousins. An electron with an energy of 20 keV, considered as low, can travel at 82,000 kilometres per second, while an electron with 1 MeV (1000 keV) of energy can go as high as

282,000 kilometres per second almost the 300,000 kilometres per second that light can travel in vacuum. When electrons travel through a transparent medium, such as glass or water, they can go faster than the speed of light for that specific medium. As a result, they emit a characteristic type of light known as Cherenkov radiation.

These electrons are known as relativistic. A complete description of their behaviour requires knowledge of Einsteins theory of relativity. Highly relativistic electrons and positrons which pass near a nucleus experience another phenomenon known as Bremsstrahlung or braking radiation. Under the influence of the nucleus intense electric field, these particles emit a gamma or X- photon which takes away some of their energy. As a result, the electron slows down. These Bremsstrahlung photons that accompany beta radiation need to be considered in radioprotection.

2.1.2 Interaction of neutral particles in a gas

One can say this as energy transfer by proxy. The neutral particles that are of interest in the field of radioactivity are gamma photons, neutrons produced in the heart of nuclear reactors, and neutrinos. These neutral particles lose their energy in a given medium by causing electrically charged particles to move. Gamma photons essentially interact with electrical charges. Neutrons are nucleons that do not feel electric charges but can nevertheless be captured by nuclei and trigger nuclear reactions such as nuclear fission.

Neutrinos are so weakly interacting that they are very difficult to detect. Practically invisible, they have a negligible effect on matter and it is therefore so easy to protect ourselves from them that we can ignore their existence. A gamma photon has the same nature as visible light. As long as the photon does not undergo a collision with an electron or a nucleus, it does not lose energy in the medium it passes through.

It also causes no damage. When it interacts, however - generally with an electron or an atom - it transfers most or all of its energy to the medium via three processes which either eject an electron away from its atom (photoelectric and Compton effects) or create a new electron and positron (pair production).

Once these electrons start moving, they lose their energy and slow down like any other charged particle. Somehow, a gamma photon outsources to these particles set in motion the task of transferring its energy to the medium. Not very localized (and therefore highly diffuse in space), it is impossible to predict where the transfer of energy will take place contrarily to the case of alpha or beta particles. Still more unpredictable is the path of a neutron, the way in which it slows down and loses its energy. A neutron completely ignores the electrons it passes, interacting only with nuclear matter. It transfer its energy by knocking nuclei and setting them in motion. It can also be captured by nuclei, often inducing nuclear reactions. After capturing one neutron, stable nuclei may become radioactive.

2.2 Ionisation Detectors

Ionization detectors were the first electrical devices developed for radiation detection. These instruments are based on the direct collection of the ionization electrons and ions produced in a gas by passing radiation. During the first half of the 20th century, three basic types of detector were developed: the ionization chamber, the proportional counter and the Geiger-Muller counter. During the late 1960's, a renewed interest in gas ionization instruments was stimulated in the particle physics domain by the invention of the multi-wire proportional chamber. These devices were capable of localizing particle trajectories to less than a millimeter and were quickly adopted in high-energy experiments. Stimulated by this success, the following years saw the

development of the drift chamber and, somewhat later, the time projection chamber. Because of their higher density, attention has also been focused on the use of liquids as an ionizing medium. The physics of ionization and transport in liquids is not as well understood as in gases, but much progress in this domain has been made and development is continuing in this area.

2.2.1 Gaseous ionisation Detectors

Because of the greater mobility of electrons and ions, a gas is the obvious medium to use for the collection of ionization from radiation. Many ionization phenomena arise in gases and over the years these have been studied and exploited in the detectors we will describe below. The three original gas devices, i.e., the ionization chamber, the proportional counter and the Geiger-Muller counter, serve as a good illustration of the application of gas ionization phenomena in this class of instruments. These detectors are actually the same device working under different operating parameters, exploiting different phenomena. Consider a chamber (Fig-2.1) with two electrodes and voltage applied across them. The chamber is filled with a suitable gas, usually a noble gas such as argon. If radiation now penetrates the chamber, a certain number of electron-ion pairs will be created, either directly, if the radiation is a charged particle, or indirectly through secondary reactions if the radiation is neutral. The mean number of pairs created is proportional to the energy deposited in the counter. Under the action of the electric field, the electrons will be accelerated towards the anode and the ions toward the cathode where they are collected.

The current signal observed, however, depends on the field intensity. This is illustrated in Fig.2.2 which plots the total charge collected as a function of V . At zero voltage, of course, no charge is collected as the ion-electron pairs recombine under their own electrical attraction. As the voltage is raised, however, the recombination

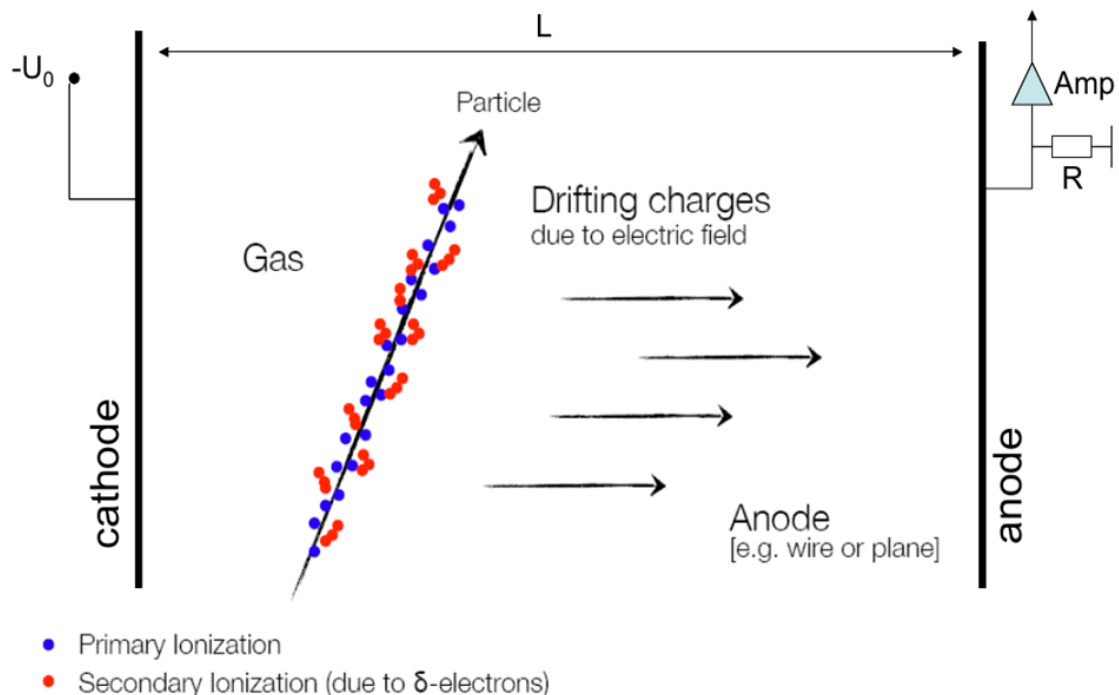


Figure 2.1: Schematic setup for a gaseous ionisation detector.

forces. are overcome and the current begins to increase as more and more of the electron-ion pairs are collected before they can recombine. At some point, of course, all created pairs will be collected and further increases in voltage show no effect. This corresponds to the first flat region in Fig.2.2 . A detector working in this region (II) is called an ionization chamber since it collects the ionization produced directly by the passing radiation. The signal current, of course, is very small and must usually be measured with an electrometer. Ionization chambers are generally used for measuring gamma ray exposure and as monitoring instruments for large fluxes of radiation. If we now increase the voltage beyond region II we find that the current increases again with the voltage. At this point, the electric field is strong enough to accelerate freed electrons to an energy where they are also capable of ionizing gas molecules in the chamber. The electrons liberated in these secondary ionisation then accelerate to produce still more ionization and so on. This results

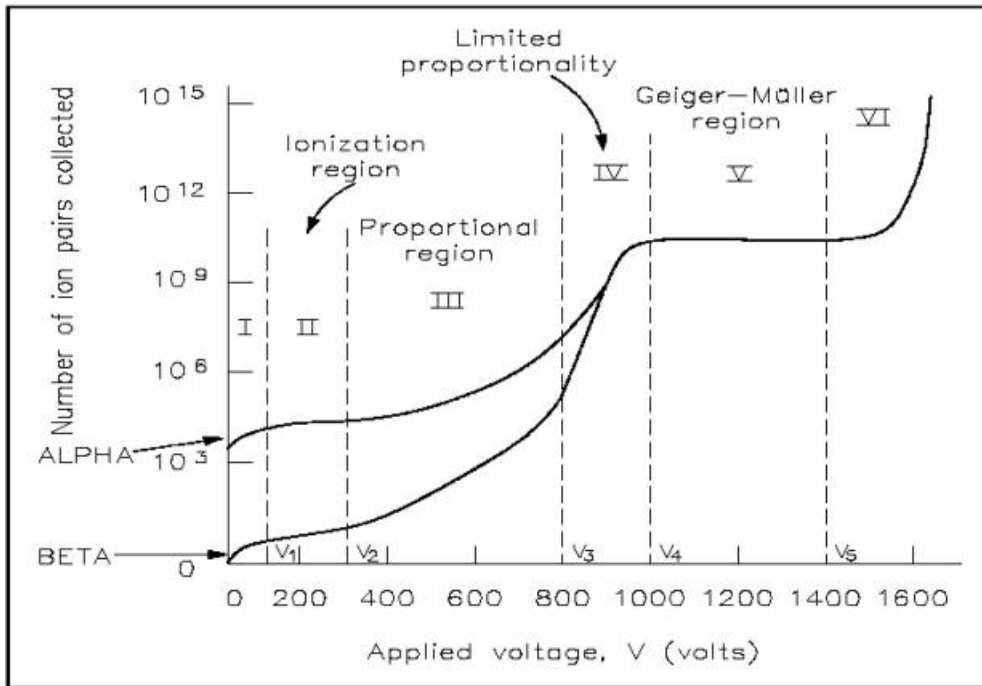


Figure 2.2: I-V characteristics of Gas detectors.

in an ionization avalanche or cascade. Since the electric field is strongest near the anode, as in most of the configurations, this avalanche occurs very quickly and almost entirely within a few millimeter from the anode. The number of electron-ion pairs in the avalanche, however, is directly proportional to the number of primary electrons. What results then is a proportional amplification of the current, with a multiplication factor depending on the working voltage V . This factor can be as high as 10^6 so that the output signal is much larger than that from an ionization chamber, but still in proportion to the original ionization produced in the detector. This region of proportional multiplication extends up to point (III) and a detector operating in this domain is known as a proportional chamber. It is the important mode for many sophisticated gas devices to be described later.

If the voltage is now increased beyond point (III), the total amount of ionization created through multiplication becomes sufficiently large that the space charge created

distorts the electric field about the anode. Proportionality thus begins to be lost. This is known as the region of limited proportionality. Increasing V still higher, the energy becomes so large that a discharge occurs in the gas. What happens physically is that instead of a single, localized avalanche at some point along the anode wire (as in a proportional counter), a chain reaction of many avalanches spread out along the entire length of the anode is triggered. These secondary avalanches are caused by photons emitted by deexciting molecules which travel to other parts of the counter to cause further ionizing events. The output current thus becomes completely saturated, always giving the same amplitude regardless of the energy of the initial event. In order to stop the discharge, a quenching gas must be present in the medium to absorb the photons and drain their energy into other channels. Detectors working in this voltage region are called Geiger-Muller or breakdown counters. The Geiger voltage region, in fact, is characterized by a plateau over which the count rate varies little. The width of the plateau depends on the efficacy of the quencher in the gas. In general, the working voltage of a Geiger counter is chosen to be in the middle of the plateau in order to minimize any variations due to voltage drift.

Finally, now, if the voltage is increased still further a continuous breakdown occurs with or without radiation. This region, of course, is to be avoided to prevent damage to the counter. In this illustration, we thus see how phenomena such as gas multiplication and discharge, in addition to gas ionization, can be used for radiation detection.

2.2.2 Choice of Gas

Two of the most important parameters for the detector performance are spatial resolution and efficiency. The resolution is directly influenced by the diffusion and the number of ionisations in the gas, whereas the efficiency only depends on the number

of ionisations. One contribution to the resolution is the diffusion $D(z)$ that goes with \sqrt{z} . Subsequently, a good resolution requires low diffusion. Many ionisations further improves the resolution. An additional requirement is the drift velocity, that is specifically important in high rate experiments; pile-up can be reduced by increasing the drift velocity.

The basic component of a gas mixture is the carrier gas. Because gas multiplication is critically dependent on the migration of free electrons rather than much slower positive ions, the fill gas in proportional counters must be chosen from those species that do not exhibit an appreciable electron attachment coefficient. Because air is not one of these, proportional counters must be designed with the provision to maintain the purity of the gas. The influence of electronegativity impurities is most pronounced in large volume counters and for small values of electron drift velocity. In CO_2 , a gas with relatively slow electron drift, it has been shown that an Oxygen concentration of 0.1% results in the loss of approximately 10% of free electrons per centimeter of travel.

A non-flammable, eco-friendly gas mixture is often a pre-requisite for safety. Hence the inert gas like Helium, Argon, Neon or Krypton can be used. These gases have the advantage that multiplication occurs already at lower fields than in other gases. But these gases have the property that they rather become excited than ionized, since their ionization energies are rather high. Since low energy transfers are more probable, the excitation reaction generally dominate. As a consequence of de-excitation, high energetic photons are created. Under proper circumstances, these photon could create additional ionization elsewhere in the fill gas through photoelectric interaction with less tightly bound electron shell or capable of ionizing the cathode, causing further avalanches. These can lead to a loss of proportionality and spurious pulses. Furthermore, they increase the possible dead time effects, reduce the spatial resolu-

tion in position sensing detector.

To avoid this, quenchers are used. Quenchers are mainly organic (polyatomic) gases, which have many non-radiative rotational and vibrational levels by which photons can be absorbed, e.g. Methane or Isobutane. Quenchers therefore help to increase the operation stability. A mixture of 90% Argon and 10% Methane is probably the most general purpose proportional gas. The ageing effect is a major problem. To clean the chamber, in general, other gases, like CF_4 , CF_3Br or alcohols like Isopropyl alcohol are used. Alcohol molecules concentrate near the anode since they have large dipole moments and will perform charge exchange with the charged ionic molecules. This will avoid their possible damage. A permanent gas circulation also slows down the process of ageing.

Even though Oxygen is electronegative, the air can serve as an acceptable proportional gas under special circumstances. If the drift distance of electron is very small and the electric field in the drift region is high enough, then electrons escape attachments to form small but detectable avalanches. Alternatively, electrons may attach O_2 molecules in the air and drift slowly to near the anode where some are detected through collision and multiplied by initiating avalanches.

2.3 Energy loss

Fast charged particles, while traveling through matter, lose kinetic energy through the following mechanism:

- 1 Coulomb Scattering: Inelastic collisions with atoms; the part of energy is transferred to excite or ionize the atoms.
- 2 Bremsstrahlung: Emission of a photon due to the deflection of the particle in the Coulomb field of a nucleus or an electron.

The heavy charged particles lose energy essentially by inelastic collision, whereas for the electrons, the bremsstrahlung starts to dominate above 10-100 MeV. For identification of the particles, we need to know the energy loss per unit distance of a moving charged particle in a medium. The mean energy loss of a particle traversing a gas volume can be calculated using the Bethe-Bloch equation. The basic assumption of Bethe-Bloch formula are:- The heavy particles interact with atomic electrons which are assumed to be free and initially at rest. It only moves very slightly during the interaction with the heavy particle. After the collision, we assume the incident particle to be essentially undeviated from its original path because of its much larger mass. The following equation gives the mean energy loss of a traversing particle along a distance

$$-\frac{dE}{dx} = 2\pi N_a n_e r_e c^2 \rho \frac{Zz^2}{A\beta_{inc}} \left[\ln \left(\frac{2m_e \gamma^2 v^2 W_{max}}{I^2} \right) - 2\beta_{inc}^2 \right] \quad (2.1)$$

where E : energy of the traversing particle ; c: velocity of light

r_e : classical electron radius ; m_e : electron mass

N_a : Avogadro's number ; I: mean excitation potential

Z: atomic number of absorbing material ; A: atomic weight of absorbing material

ρ : density of absorbing material ; z: charge of incident particle

β_{inc} : $\frac{v}{c}$ of the incident particle & γ : $\frac{1}{\sqrt{1-\beta_{inc}^2}}$

W_{max} : maximum energy transfer in a single collision

Bethe-Bloch formula for the energy loss of a charged particle in a medium is well known but gives only the mean integrated energy loss. The energy loss is however a statistical process and will, therefore, fluctuate from event to event. To simulate the true signal in a proportional chamber, it is necessary to use a much more detailed model that gives the distribution of the individual ionization along the track and their

energies. The photo absorption ionization (PAI) model is one of the such models. It was developed using a semiclassical approach. In the simulation programme HEED, this PAI model is used for the calculation of the ionization and cluster formation. An effective description of the ionization left by the particle along its trajectory is provided by a probability distribution of the number electrons liberated directly or indirectly with each primary encounter. It is known as cluster size distribution. For most of the primary ionizing collisions, the energy transfers are small. As a result the secondary ionization is produced close to the primary collisions and the total ionization along the particle tracks appears in clusters.

2.4 Different types of ionisation mechanism

The main interactions of charged particles with matter are ionisation and excitation. For relativistic particles, bremsstrahlung energy losses must also be considered. Neutral particles must produce charged particles in an interaction that are then detected via their characteristic interaction processes. In the case of photons, these processes are the photoelectric effect, Compton scattering and pair production of electrons. The electrons produced in these photon interactions can be observed through their ionisation in the sensitive volume of the detector.

When the incident particle passes through matter, it transfers a part of its energy to atoms through collisions with them. This energy is dissipated in matter by emission of a series of electrons and photons which ionize other atoms and so on. Different processes, that can take place, are described below with symbols :-

Primary processes :-

excitation: $X \rightarrow X^*$

ionization: $X \rightarrow X^+ + e^-$

dissociation: $X \rightarrow Y^* + Z^*$

elastic collision: $X \rightarrow X$

Now using these many types of secondary process can also occur as following

secondary processes :-

non-radiative transitions: $X^* + Y \rightarrow X + Y^*$

radiative transitions: $X^* \rightarrow X + h\nu$

Penning effect: $X^* + Y \rightarrow X + Y^+ + e^-$

charge exchange: $X^+ + Y \rightarrow X + Y^+$

electron capture: $X + e^- \rightarrow X^- + h\nu$

recombination: $X^+ + e^- \rightarrow X + h\nu$

secondary ionization: $e^- + X \rightarrow X^+ + 2e^-$

Some of the processes are described in detail later.

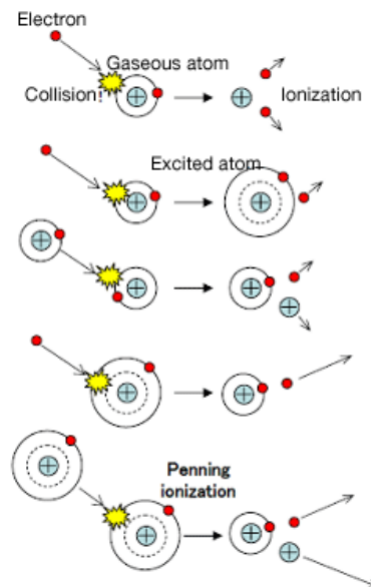


Figure 2.3: Ionisation mechanisms considering Bohr's model of an atom.

Chapter 3

Energy loss of Charged Particles

3.1 Bethe-Bloch formula

Let us discuss an approximate derivation. In this way, the physical meaning of the terms appearing in the formula and their behavior as a function of incoming velocity become more evident. We restrict ourselves to cases where only a small fraction of the incoming kinetic energy is transferred to atomic electrons, so that the incoming particle trajectory is not deviated. Now, we introduce the impact parameter b describing how close the collision is : b is the minimal distance of the incoming particle to the target electron. In general, large values of b correspond to the so-called distant collisions, conversely small values to close collisions. Both kinds of collisions are important for determining the average energy-loss [Eq. 2.1], the energy straggling (i.e., the energy-loss distribution) and the most probable energy-loss. When a particle of charge z_1e , mass M and velocity v interacts with a particle in the material with mass m , charge z_2e and we assume that, to a first approximation, the material particle will emerge only after the particle passage so that we can consider the electron essentially at rest throughout the interaction. We restrict ourselves to cases where only small momentum transfers are involved, so that the trajectory of the incident particle is not appreciably altered and the material particle only has a small recoil. The trajectory of the incident particle defines the axis of a cylinder as shown in fig:- We consider the interaction with a particle in the cylindrical shell a distance b from the axis. The distance b is referred to as the impact parameter for the interaction.

The moving charge creates an electric and magnetic field at the location of the ma-

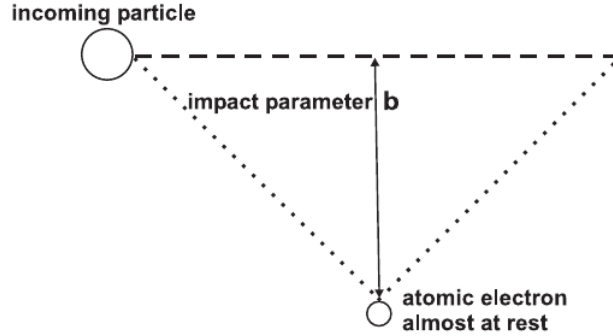


Figure 3.1: Incoming fast particle of charge ze scattered by an atomic electron almost at rest: for small energy transfer, the particle trajectory is not deflected

terial particle. Since the material particle is assumed to have only a small velocity, the magnetic interaction is not important. By symmetry the net force acting on the material particle is perpendicular to the cylinder.

The transverse electric field is

$$E_{\perp} = \frac{z_1 e b}{r^3} \quad (3.1)$$

in the rest frame of the incident particle. The electric field observed in the LAB changes with time. Suppose that the incident particle reaches its pointy of closest approach at $t = 0$. At time t the transeverse electric field in LAB frame is given by [18]

$$E_{\perp} = \frac{\gamma z_1 e b}{(b^2 + \gamma^2 v^2 t^2)^{3/2}} \quad (3.2)$$

The momentum acquired by the bound particle is

$$\Delta p = \int F dt = \int_{-\infty}^{\infty} \frac{(z_2 e) \gamma z_1 e b}{(b^2 + \gamma^2 v^2 t^2)^{3/2}} dt = \frac{2 z_1 z_2 e^2}{v b} \quad (3.3)$$

The incident particle will have collisions with both the nuclei and the electrons of the atoms. Since the bound particle is assumed to have only a small velocity,

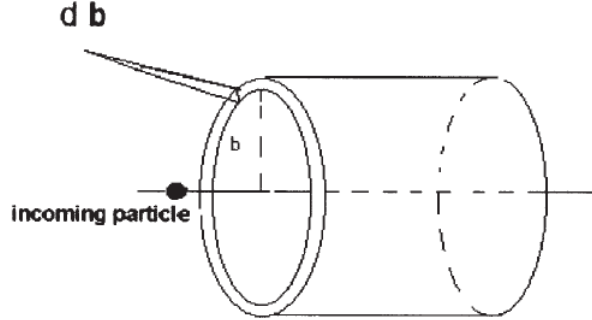


Figure 3.2: An incoming fast particle of charge ze interacts with electrons at impact parameter between b and $b + db$

the energy transefer can be written (caution same symbol used for electric field and energy, clear from the context)

$$\Delta E = \frac{(\Delta p)^2}{2m} = \frac{2z_1^2 z_2^2 e^4}{b^2 v^2 m} \quad (3.4)$$

Inverse relation with the impact parameters says that most of the energy transefer is due to close collisions. We have $m = m_e$ and $z_2 = 1$ for electrons and $m = Am_p$ and $z_2 = Z$ for nuclei. With Z electrons in an atom and $A \approx 2Z$,

$$\frac{\Delta E(\text{electrons})}{\Delta E(\text{nucleus})} = \frac{Z}{m_e} \left(\frac{Z^2}{2Zm_p} \right)^{-1} \approx 4000 \quad (3.5)$$

so we see that the atomic electrons are responsible for most of the energy loss. We will let $m = m_e$ for rest of the disscusion.

Now let us calculate the total energy lost by the incident particle per unit length in the material. We have just seen that most of the energy loss is due to interactions with the atomic electrons. There are $n_e \times 2\pi b db dx$ electrons in the cylindrical shell of Figure(3.2), where

$$n_e = z_2 n_a = z_2 \frac{N_a \rho}{A} \quad (3.6)$$

is the number of the electrons per unit volume. Summing over the total energy transfer in each b interval, the total energy loss per unit length is

$$-\frac{dE}{dx} = 2\pi n_e \left(\frac{2z_1^2 e^4}{mv^2} \right) \int_{b_{min}}^{b_{max}} \frac{db}{b} = \frac{4\pi n_e z_1^2 e^4}{mv^2} \ln \frac{b_{max}}{b_{min}} \quad (3.7)$$

The limiting values of the impact parameter are determined by the range of validity of the various assumptions that were made in deriving last equation. We have assumed that the interaction takes place between the electric field of the incident particle and a free electron. However, the electron is actually bound to an atom. The interaction may be considered to be with a free electron only if the collision time is too short compared to the characteristic orbital period of electrons in the atom. Examination of Eq. 3.2 shows that the transeverse electric field in the LAB is very small except near $t = 0$. The full width at half maximum of the electric field $E(t)$ distribution is $\frac{b}{v\gamma}$ times a constant of order 1, so we take [18]

$$t_{coll} \simeq \frac{b}{v\gamma} \quad (3.8)$$

An upper limit for the impact parameter then is

$$b_{max} \simeq \frac{\gamma v}{\omega} = \frac{\gamma v h}{I} \quad (3.9)$$

where ω is a characteristic orbital frequency and $I = h\omega$ is the mean excitation energy. The lower limit b_{min} is evaluated considering the extent to which the classical treatment can be employed. In the framework of the classical approach, the wave characteristics of particles are neglected. This assumption is valid as long as the impact parameter is larger than the de Broglie wavelength of the electron in the center-of-mass system (CoMS) of the interaction. For instance, we can assume

$$b_{min} \simeq \frac{h}{2P_{eCM}} \quad (3.10)$$

where P_{eCM} is the electron momentum in the CoMS. Because the electron mass is much smaller than the mass of the incoming heavy-particle, the CoMS is approximately associated with the incoming particle and conversely the electron velocity in the CoMS is opposite and almost equal in absolute value to that of the incoming particle, v . Thus, we have that

$$|P_{eCM}| \simeq m\gamma v = m\gamma\beta c \quad (3.11)$$

and substituting in equation-3.7 we obtain:

$$-\frac{dE}{dx} = \frac{4\pi n_e z_1^2 e^4}{mv^2} \ln \left[\left(\frac{vh\gamma}{I} \right) \left(\frac{2m\gamma\beta c}{h} \right) \right] = \frac{2\pi n z^2 e^4}{mv^2} \ln \left(\frac{2m\gamma^2 v^2}{I} \right)^2 \quad (3.12)$$

Finally, using the value of the maximum energy transfer $W_m = 2mv^2\gamma^2$ from two body scattering we get:

$$-\frac{dE}{dx} = \frac{2\pi n z^2 e^4}{mv^2} \ln \left[\frac{2m\gamma^2 v^2 W_m}{I^2} \right] \quad (3.13)$$

This equation is equivalent to the energy-loss formula except for the terms $2\beta^2$, $-\delta$ due to the density-effect and the shell correction term ($-U$). When the first of these latter terms is added, we obtain the expression (termed Bethe relativistic formula)

$$-\frac{dE}{dx} = \frac{4\pi n z^2 e^4}{mv^2} \left(\ln \left[\frac{2m\gamma^2 v^2}{I} \right] - \beta^2 \right) \quad (3.14)$$

derived in the quantum treatment of energy loss by collisions of a heavy, spin-0 incident particle.

Furthermore, it has to be noted that spin plays an important role when the transferred energy is almost equal to the incoming energy (this occurs with very limited statistical probability). At low particle velocity [the energy-loss process due to Coulomb interactions on nuclei (termed nuclear energy-loss and resulting in the nuclear stopping

power) cannot be neglected], additional corrections are added: for instance, corrections accounting for the Barkas effect [denotes the observed difference in ranges of positive and negative particles in emulsion] and the Bloch correction[derives from the Bloch quantum-mechanical approach in which he did not assume, unlike Bethe, that it is valid to consider the electrons to be represented by plane waves in the center-of-momentum reference frame].

Chapter 4

Transport of charged particle in Gases

A charged particle under the effect of an electric field is accelerated along the field lines. Here the drift velocity of electrons & ions and the diffusion of electrons are described. To model the slowing down of the drifting particles by the gas molecules, a friction force, proportional to the velocity, has been introduced. The behaviour of the drift chamber is crucially dependent on the drift of the electrons and ions that are created by the particles measured or in the avalanches at the electrodes. In addition to the electric drift field, there is often a magnetic field, which is necessary for measuring particle momentum. Obviously we have to understand how the drift velocity vector in electric and magnetic fields depends on the properties of the gas molecules, including their density and temperature.

Differences in behaviour of ions and electrons : As might be expected, electrons usually have much higher drift velocities and diffusion coefficients (by orders of magnitude) than ions under given conditions in a given gas. Because of their small mass, electrons are accelerated rapidly by an electric field, and they lose little energy in elastic collisions with molecules (a fraction of the order of m_e/M , where m_e and M are the electronic and molecular masses, respectively.) Therefore, electrons can acquire kinetic energy from an electric field faster than ions, and they can store this energy between collisions to a much greater degree until they reach energies at which inelastic collisions become important. Even with only a weak electric field imposed on the gas through which the electrons are moving, the average electronic energy may be far in excess of the thermal value associated with the gas molecules. Furthermore,

the electronic energy distribution is not close to Maxwellian except at extremely low values of E/N .

Other differences between electrons and ions develop in connection with their collision cross sections. Electronic excitation of atoms and molecules is frequently an important factor in electron collisions even for impact energies of less than 10 eV, and in molecular gases the onset of vibrational and rotational excitation occurs at energies far below 1 eV. These energies are often attained by electrons in situations of common interest. The laboratory-frame thresholds for the corresponding modes of excitation by ions are higher than those for electrons, and the excitation cross sections peak at energies considerably above these thresholds. Therefore, ions have insufficient energy to produce much excitation under the usual gas kinetic conditions. These considerations tend to make the analysis of electronic motion in gases more difficult than the analysis of ionic motion. A compensating factor is operative, however, because of the relatively small mass of the electron. Since $m_e/M \ll 1$ in any gas, it is possible to make approximations in the analysis of electronic motion that are not valid in the ionic case. These approximations greatly simplify the mathematics and make it possible to calculate accurately the velocity distribution and transport properties of electrons in many gases at high E/N . This is not so with ions.

On the experimental side certain other important differences appear. Electrons may be produced much more simply than ions by thermionic emission from filaments, by photoemission from surfaces, or by beta decay of radioactive isotopes. Ionic production usually requires the use of much more elaborate apparatus: electron bombardment or photoionization ion sources or an electrical discharge. Furthermore, in an electron-swarm experiment the electronic component of the charge carriers may be easily separated from any ionic component that may be present and no mass analysis is required to interpret the data. In ionic drift and diffusion experiments, on

the other hand, mass analysis of the ions is usually essential if unambiguous results are to be obtained. This requirement involves a great complication of the apparatus. On the other hand, electron swarm experiments are usually more sensitive than ion experiments to electric field non uniformities, contact potentials, and magnetic fields.

A final difference between electron and ion experiments relates to the effects of impurities in the gas being studied. Molecular impurities in an atomic gas can hold the average electronic energy well below the level that would be attained in the pure gas because electrons can lose large fractions of their energy by exciting the rotational and vibrational levels of the molecules. The electronic velocity distribution can be seriously altered in the process. In ionic experiments, however, impurities have little effect on the average ionic energy and velocity distribution. The complication that may develop instead is the production of impurity ions by the reaction of the ions of the main gas with impurity molecules. This is frequently a matter of serious concern.

4.1 Drift of Charged Particle

The motion of charged particles under the influence of electric and magnetic fields obey the following equation of motion :

$$m \frac{d\vec{u}}{dt} = q\vec{E} + q(\vec{u} \times \vec{B}) - f\vec{u} \quad (4.1)$$

where m and q are the mass and electric charge of the particle, u is its velocity vector, and f describes a frictional force proportional to u that is caused by the interaction of the particle with the gas. This equation describes the drift at large t to a very good approximation. This was introduced by P. Langevin, who imagined the force $f u$ as a stochastic average over the random collisions of the drifting particle. The ratio m/f has the dimension of a characteristic time, and we define $\tau = m/f$. For very large time $t \gg \tau$ we will get a steady state solution with $\frac{d\vec{u}}{dt} = 0$. So we get the linear

differential equation for the drift velocity vector as

$$\frac{1}{\tau}\vec{u} - \frac{q}{m}[\vec{u} \times \vec{B}] = \frac{q}{m}\vec{E} \quad (4.2)$$

In order to solve for \vec{u} , we write $(q/m)B_x = \omega_x$ etc., $(q/m)E_x = \epsilon_x$ etc., and express the above equation in the form of the matrix equation

$$\mathbf{M}\mathbf{u} = \epsilon \quad (4.3)$$

where

$$M = \begin{bmatrix} 1/\tau & -\omega_z & \omega_y \\ \omega_z & 1/\tau & -\omega_x \\ -\omega_y & \omega_x & 1/\tau \end{bmatrix}$$

After inverting the matrix we get the solution for the drift velocity as

$$\vec{u} = M^{-1}\vec{\epsilon} = \begin{bmatrix} 1 + \omega_x^2\tau^2 & \omega_z\tau + \omega_x\omega_y\tau^2 & -\omega_y\tau + \omega_x\omega_z\tau^2 \\ -\omega_z\tau + \omega_x\omega_y\tau^2 & 1 + \omega_y^2\tau^2 & \omega_x\tau + \omega_y\omega_z\tau^2 \\ \omega_y\tau + \omega_x\omega_z\tau^2 & -\omega_x\tau + \omega_y\omega_z\tau^2 & 1 + \omega_z^2\tau^2 \end{bmatrix} \times \frac{\tau}{1 + \omega^2\tau^2}\vec{\epsilon} \quad (4.4)$$

where $\omega^2 = \omega_x^2 + \omega_y^2 + \omega_z^2 = (q/m)^2B^2$ is the square of the cyclotron frequency of the electron. We can write the same equation as

$$\vec{u} = \frac{q}{m}|\mathbf{E}|\frac{\tau}{1 + \omega^2\tau^2} \left(\hat{E} + \omega\tau[\hat{E} \times \hat{B}] + \omega^2\tau^2(\hat{E} \cdot \hat{B})\hat{B} \right) \quad (4.5)$$

Here \hat{E} and \hat{B} denote the unit vectors in the directions of the fields. The drift direction is governed by the dimensionless parameter $\omega\tau$, where ω is defined as $(q/m)|B|$ and carries the sign of the charge of the moving particle. For $\omega\tau = 0$, \vec{u} is along \vec{E} ; in this case the relation has the simple form

$$\vec{u} = \frac{q}{m}\tau\vec{E} = \mu\vec{E} \quad (4.6)$$

where $\mu = \frac{q}{m}\tau$ is defined as the scalar mobility, the ratio of drift velocity to electric field in the absence of magnetic field; μ is proportional to the characteristic time τ and carries the charge sign of the particle.

In the presence of the magnetic field, the mobility is the tensor $(q/m)M^{-1}$ given in Eq-4.4 . For large positive values of $\omega\tau$ and $q > 0$, \vec{u} generally tends to be along \vec{B} ; but if $\hat{E} \cdot \hat{B} = 0$, then large $\omega\tau$ turn \vec{u} in the direction of $\hat{E} \times \hat{B}$, independently of the sign of q . Both the direction and the magnitude of u are influenced by the magnetic field. If we distinguish $u(\omega)$, the drift velocity in the presence of B , and $u(0)$, the drift velocity at $B = 0$ under otherwise identical circumstances, using eq-5 we derive

$$\frac{u^2(\omega)}{u^2(0)} = \frac{1 + \omega^2\tau^2 \cos^2\phi}{1 + \omega^2\tau^2} \quad (4.7)$$

where ϕ is the angle between E and B . This ratio happens to be the same as the one by which the component of u along E , u_E , changes with B :

$$\frac{u_E(\omega)}{u_E(0)} = \frac{1 + \omega^2\tau^2 \cos^2\phi}{1 + \omega^2\tau^2} \quad (4.8)$$

4.2 Microscopic Picture

When charges drifting through the gas are scattered on the gas molecules so that their direction of motion is randomized in each collision. On average, they assume a constant drift velocity \vec{u} in the direction of the electric field (or, if a magnetic field is also present, in the direction which is given by both fields). The drift velocity is much smaller than the instantaneous velocity c between collisions. The gases we deal with are sufficiently rarefied that the distances travelled by electrons between collisions are large in comparison with their Compton wavelengths. So our picture is classical and atomistic.

4.2.1 Drift of Electrons

Consider an electron moving between two successive collisions. Because of its light mass, the electron scatters isotropically and, immediately after the collision, it has

forgotten any preferential direction. Some short time later, in addition to its instantaneous and randomly oriented velocity c , the electron has picked up the extra velocity u equal to its acceleration along the field, multiplied by the average time that has elapsed since the last collision:

$$\vec{u} = \frac{e\vec{E}}{m}\tau \quad (4.9)$$

This extra velocity appears macroscopically as the drift velocity. In the next encounter, the extra energy, on the average, is lost in the collision through recoil or excitation. Therefore there is a balance between the energy picked up and the collision losses. On a drift distance x , the number of encounters is $n = (x/u)(1/\tau)$, the time of the drift divided by the average time τ between collisions. If λ denotes the average fractional energy loss per collision, the energy balance is the following:

$$\frac{x}{u\tau}\lambda\epsilon_E = eEx \quad (4.10)$$

Here the equilibrium energy ϵ_E carries an index E because it does not contain the part due to the thermal motion of the gas molecules, but only the part taken out of the electric field.

We have the average time between collisions same as the average time that has elapsed since the last collision. This is because in a completely random series of encounters, characterized only by the average rate $1/\tau$, the differential probability $f(t)dt$ that the next encounter is a time between t and $t + dt$ away from any given point $t = 0$ in time is

$$f(t)dt = 1/\tau e^{-t/\tau} dt \quad (4.11)$$

independent of the point where the time measurement begins. In the frictional-motion picture, τ was the ratio of the mass of the drifting particle over the coefficient of friction. In the microscopic picture, τ is the mean time between the collisions of the

drifting particle with the atoms of the gas. For drifting particles with instantaneous velocity c , the mean time τ between collisions may be expressed in terms of the cross-section σ and the number density N :

$$\frac{1}{\tau} = N\sigma c \quad (4.12)$$

Here c is related to the total energy of the drifting electron by

$$\frac{1}{2}mc^2 = \varepsilon = \varepsilon_E + \frac{3}{2}kT \quad (4.13)$$

because the total energy is made up of two parts: the energy received from the electric field and the thermal energy that is appropriate for 3 degrees of freedom ($k =$ Boltzmanns constant, $T =$ gas temperature). For electron drift in particle detectors, we usually have $\varepsilon_E \gg (3/2)kT$; we can neglect the thermal motion, and eq- 4.9,4.10&4.13 combine to give the two equilibrium velocities as follows:

$$u^2 = \frac{eE}{mN\sigma} \sqrt{\frac{\lambda}{2}} \quad (4.14)$$

$$c^2 = \frac{eE}{mN\sigma} \sqrt{\frac{2}{\lambda}} \quad (4.15)$$

where $\varepsilon = (1/2)mc^2 \simeq \varepsilon_E \gg (3/2)kT$

4.3 Drift of Ions

The behavior of ions differs from that of electrons because of their much larger mass and their chemical reactions. Electrons in an electric field are accelerated more rapidly than ions, and they lose very little energy when colliding elastically with the gas atoms. The electron momentum is randomized in the collisions and is therefore lost, on the average. In electric field strengths that are typical for drift chambers, the electrons reach random energies far in excess of the energy of the thermal motion, and quite often they surpass the threshold of inelastic excitation of molecules in the

gas. In this case their mobility becomes a function of the energy loss that is associated with such excitation. Ions in similar fields acquire, on one mean-free path, an amount of energy that is similar to that acquired by electrons. But a good fraction of this energy is lost in the next collision, and the ion momentum is not randomized as much. Therefore, far less field energy is stored in random motion. As a consequence, the random energy of ions is mostly thermal, and only a small fraction is due to the field. The effect on the diffusion of ions results in this diffusion being orders of magnitude smaller than that of electrons in similar fields. The effect on the mobility is also quite interesting: since the energy scale, over which collision cross-sections vary significantly, is easily covered by the electron random energies reached under various operating conditions, we find rapid and sometimes complicated dependencies of electron mobility on such operating conditions electric and magnetic field strengths and gas composition being examples. In contrast, the mobility of ions does not vary as much.

4.4 Inclusion of Magnetic Field

When we consider the influence of a magnetic field on drifting electrons and ions, the first indication may be provided by the value of the mobility of these charges. In particle chamber conditions, this is of the order of magnitude of $\mu \simeq 10^4 \text{cm}^2 \text{V}^{-1} \text{s}^{-1}$ for electrons whereas for ions the order of magnitude is $\mu = 1 \text{cm}^2 \text{V}^{-1} \text{s}^{-1}$. Now it is the numerical value of $\omega\tau = (e/m)B\tau$ that governs the effects of the magnetic field on the drift velocity vector.

Therefore, the effect of such magnetic fields on ion drift is negligible, and we concentrate on electrons. This has the advantage that we may assume that the colliding body scatters isotropically in all directions, owing to its small mass.

When the magnetic field is added we can describe the most general case in a coordinate system in which B is along z , and E has components E_z and E_x . An electron between collisions moves according to the equation of motion,

$$m \frac{d\vec{v}}{dt} = q\vec{E} + q(\vec{v} \times \vec{B}) \quad (4.16)$$

so we are getting

$$\begin{aligned} \dot{v}_x &= \epsilon_x + \omega v_y \\ \dot{v}_y &= -\omega v_x \\ \dot{v}_z &= \epsilon_z \end{aligned} \quad (4.17)$$

Electrons have their direction of motion randomized in each collision, and we are interested in the extra velocity picked up by the electron since the last collision. Hence we look for the solution of eq-4.16 with $v = 0$ at $t = 0$. It is given by

$$\begin{aligned} v_x &= (\epsilon_x/\omega) \sin \omega t \\ v_y &= (\epsilon_y/\omega) (\cos \omega t - 1) \\ v_z &= \epsilon_z t \end{aligned} \quad (4.18)$$

Before we can identify v with the drift velocity u , we must average over t , using (4.11), the probability distribution of t . This was also done when deriving (4.9), which, being a linear function of time, required t to be replaced by τ , the mean time since the last collision. The drift velocity for the present case is given by

$$\begin{aligned} u_x = \langle v_x(t) \rangle &= \frac{\epsilon_x}{\omega} \int_0^\infty \frac{1}{\tau} e^{-t/\tau} \sin(\omega t) dt = \frac{\epsilon_x \tau}{1 + \omega^2 \tau^2} \\ u_y = \langle v_y(t) \rangle &= \frac{\epsilon_x}{\omega} \int_0^\infty \frac{1}{\tau} e^{-t/\tau} \sin(\omega t) dt = \frac{\epsilon_x \omega \tau^2}{1 + \omega^2 \tau^2} \\ u_z = \langle v_z(t) \rangle &= \frac{\epsilon_z}{\omega} \int_0^\infty \frac{1}{\tau} e^{-t/\tau} dt = \epsilon_z \tau \end{aligned} \quad (4.19)$$

4.5 Diffusion

A charged particle drifting under the influence of external fields scatters off the gas molecules and does not follow precisely the field lines. A cloud of such particles spread

out perpendicular and along the field lines. This process is called diffusion. After a collision, ions retain their direction of motion to some extent because their mass is comparable to the mass of the gas molecules. These diffuse little at the typical drift fields encountered in gas detectors. Electrons, scatter almost isotropically and their direction of motion is randomized after each collision. As the drifting electrons or ions are scattered on the gas molecules, their drift velocity deviates from the average owing to the random nature of the collisions. In the simplest case the deviation is the same in all directions, and a point-like cloud of electrons which then begins to drift at time $t = 0$ from the origin in the z direction will, after some time t , assume the following Gaussian density distribution:

$$n(r, t) = \left(\frac{1}{4\pi Dt} \right)^{3/2} \exp\left(\frac{-r^2}{4Dt} \right) \quad (4.20)$$

where

$$r^2 = x^2 + y^2 + (z - ut)^2$$

D is the diffusion constant because n satisfies the continuity equation for the conserved electron current density Γ (it has both drift and diffusion current):

$$\Gamma = nu - D\nabla n \quad (4.21)$$

For a detailed explanation of the solution of diffusion equation we will go through the Fick's laws and some mathematical physics to solve the differential equation. Diffusion is the process by which an uneven concentration of a substance gets gradually smoothed out spontaneously. e.g., a concentration of a chemical species (like a drop of ink or dye) in a beaker of water spreads out by itself, even in the absence of stirring. The microscopic mechanism of diffusion involves a very large number of collisions of the dye molecules with those of the fluid, which cause the dye molecules to move essentially randomly and disperse throughout the medium, even without any stirring of

the fluid. A macroscopic description of the process is based on Ficks Laws, and leads to a fundamental partial differential equation, the diffusion equation. This equation serves as a basic model of phenomena that exhibit dissipation, a consequence of the irreversibility of macroscopic systems in time. The local, instantaneous concentration $n(r, t)$ of electron swarm satisfies the equation of continuity, which is called Ficks first law in this context:

$$\frac{\partial n}{\partial t} + \nabla \cdot \Gamma = 0 \quad (4.22)$$

We assume that j is proportional to the local difference in concentrations, i.e., to the gradient of the concentration itself. Thus

$$\Gamma = -D\nabla n \quad (4.23)$$

The minus sign on the right-hand side signifies the fact that the diffusion occurs from a region of higher concentration to a region of lower concentration: That is, the diffusion current tends to make the concentration uniform. Eliminating Γ , we get the diffusion equation for the concentration $n(r, t)$:

$$\frac{\partial n}{\partial t} = D\nabla^2 n \quad (4.24)$$

This equation is of first order in the time variable, and second order in the spatial variables. It is a parabolic equation in the standard classification of second-order partial differential equations. In order to find a unique solution to it, you need an initial condition that specifies the initial concentration profile $n(r, 0)$, as well as boundary conditions that specify $n(r, t)$, for all $t \geq 0$, at the boundaries of the region in which the diffusion is taking place. The presence of the first-order time derivative in the diffusion equation implies that the equation is not invariant under the time reversal transformation $t \mapsto -t$. Irreversibility is thus built into the description of the phenomenon.

For the fundamental solution in 3 dimensions, we begin with the (eq-4.24) and the initial and boundary conditions where $n(r, t)$ satisfies natural boundary conditions, i.e., $n(r, t) \rightarrow 0$ as $r \rightarrow \infty$ along any direction. We may start with the initial condition $n(r, 0) = \delta(r)$. This means that the diffusing particle starts at the origin at $t = 0$. In the context of the diffusion equation for the concentration $n(r, t)$, such an initial condition represents a point source of unit concentration at the origin. In a space of infinite extent, we may take the starting point to be the origin of coordinates without any loss of generality. The solution thus obtained is the fundamental solution (or Green function) of the diffusion equation. The diffusion equation presents an initial value problem. Moreover, it is a linear equation in the unknown function $n(r, t)$. It is therefore well-suited to the application of Laplace transforms (with respect to the time variable). As far as the spatial variable r is concerned, it is natural to use Fourier transforms.

Taking the Laplace transform of both sides of the diffusion equation, we get

$$\begin{aligned} s\tilde{n}(r, s) - n(r, 0) &= D\nabla^2\tilde{n}(r, s) \\ \Rightarrow (s - D\nabla^2)\tilde{n}(r, s) &= \delta(r) \end{aligned} \tag{4.25}$$

where $\tilde{n}(r, s) = \int_0^\infty dt e^{-st} n(r, t)$, the Laplace transform of $n(r, t)$;

Now expand $\tilde{n}(r, s)$ in a Fourier integral with respect to the spatial variable r , according to

$$\begin{aligned} \tilde{n}(r, s) &= \frac{1}{(2\pi)^3} \int d^3k e^{ik \cdot r} \tilde{p}(k, s) \\ \tilde{p}(k, s) &= \int d^3r e^{-ik \cdot r} \tilde{n}(r, s) \end{aligned}$$

so using these expressions in the eq-4.25 for $\tilde{n}(r, s)$ and equate the coefficients of the

basis vector $e^{ik \cdot r}$ in the space of functions of r . We must then have, for each k ,

$$\begin{aligned} (s + Dk^2)\tilde{p}(k, s) &= 1 \\ \Rightarrow \tilde{p}(k, s) &= \frac{1}{s + Dk^2} \end{aligned}$$

We got 1 on the right side by taking the Fourier transform of the delta function of eq-4.25. We thus obtain a very simple expression for the double transform $\tilde{p}(k, s)$. The transforms must be inverted to find the $n(r, t)$. It is easier to invert the Laplace transform first, and then the Fourier transform. The Laplace transform is trivially inverted, as we have

$$\mathcal{L}^{-1}[1/(s + a)] = e^{-at}$$

. Therefore

$$p(k, t) = e^{-Dk^2 t} \tag{4.26}$$

and we will have the solution by taking the inverse Fourier transform of $p(k, t)$

$$n(r, t) = \frac{1}{(2\pi)^3} \int d^3k e^{ik \cdot r} e^{-Dk^2 t} \tag{4.27}$$

This 3D integral factors into a product of 3 integrals upon writing r and k in Cartesian coordinates. Each of the factors is the familiar shifted Gaussian integral. For 1D it looks like

$$n(x, t) = \frac{1}{2\pi} \int_{-\infty}^{\infty} dk_x e^{ik_x \cdot x} e^{-Dk_x^2 t} \tag{4.28}$$

By completing the square of the exponential part we get the solution

$$n(x, t) = \left(\frac{1}{4\pi Dt} \right)^{1/2} \exp\left(\frac{-x^2}{4Dt} \right) \tag{4.29}$$

For the solution (eq-4.27) we have to multiply 3 of the these and we get eq-4.20 where we have relaced z by $z - ut$ to consider the drift in z -direction.

From microscopic picture it comes out to be that the diffusion constant

$$D = \frac{l_0^2}{3\tau} = \frac{c^2\tau}{3} = \frac{2\varepsilon}{3m}\tau = \frac{2\varepsilon\mu}{3e} \tag{4.30}$$

We have used the expression for the electron mobility, where $l_0 = c\tau$ is the mean free path.

When the diffusing body has thermal energy, $\varepsilon = (3/2)kT$ we get the Einstein formula stated above in (eq-3.4). The diffusion constant D , defined by (3.25), makes the mean squared deviation of the electrons equal to $2Dt$ in any one direction from their centre. The energy determines the diffusion width σ_x of an electron cloud which, after starting point-like, has travelled over a distance L :

$$\sigma_x^2 = 2Dt = \frac{2DL}{\mu E} = \frac{4\varepsilon L}{3eE} \quad (4.31)$$

In drift chambers we therefore require small electron energies at high drift fields in order to have σ_x^2 as small as possible.

4.6 Electric Anisotropy

After some experimental evidence in 1967 the assumption of the isotropic form of diffusion constant was considered seriously. Experimentally it was shown that the value of electron diffusion along the electric field can be quite different from that in the perpendicular direction. The diffusion of drifting ions is also often found to be non-isotropic. The value of electron diffusion along the electric field can be quite different from that in the perpendicular direction. The diffusion of drifting ions is also often found to be non-isotropic.

When ions collide with the gas molecules, they retain their direction of motion to some extent because the masses of the two collision partners are similar, and therefore the instantaneous velocity has a preferential direction along the electric field. This causes the diffusion to be larger in the drift direction; the mechanism is at work for ions travelling in high electric fields $E[eE/(N\sigma) \gtrsim kT]$, and we do not treat it here because it plays no role in the detection of particles. In the case of electrons, there

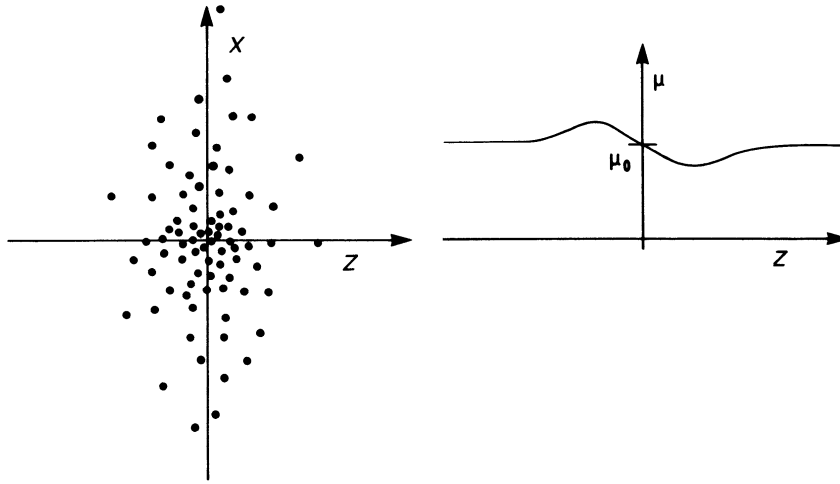


Figure 4.1: Mobility variation inside an electron cloud travelling in the z direction.

is almost no preferential direction for the instantaneous velocity. We will look at the electron diffusion anisotropy qualitatively. The essential point of the argument is that the mobility of the electrons assumes different values in the leading edge and in the centre of the travelling cloud if the collision rate is a function of electron energy. This change of mobility inside the cloud is equivalent to a change of diffusion in the longitudinal direction. Instead of the density distribution (4.20) of the diffusing cloud of electrons, we get in the anisotropic case

$$n = \frac{1}{\sqrt{4\pi D_L t}} \left(\frac{1}{4\pi D_T t} \right) \exp \left[-\frac{x^2 + y^2}{4D_T t} - \frac{(z - ut)^2}{4D_L t} \right] \quad (4.32)$$

4.7 Magnetic Anisotropy

Let us now consider the effect of a magnetic field B along z . The electric field is in the $x - z$ plane and we assume there is no electric anisotropy. The magnetic field causes the electrons to move in helices rather than in straight lines between collisions.

Projection onto the $x - y$ plane yields circles with radii

$$\rho = \frac{c}{\omega} \sin\theta \quad (4.33)$$

the magnetic field has caused the diffusion along x and y (then perpendicular to the magnetic field) to be reduced by the factor

$$\frac{D_T(\omega)}{D_T(0)} = \frac{1}{1 + \omega^2 \tau^2} \quad (4.34)$$

whereas the longitudinal diffusion is the same as before:

$$D_L(\omega) = D_L(0) \quad (4.35)$$

If there is an E field as well as a B field in the gas, the electric and magnetic anisotropies combine. In the most general case of arbitrary field directions, the diffusion is described by a 3×3 tensor. The diffusion tensor must be positive definite, otherwise our cloud would shrink in some direction a thermodynamic impossibility.

4.8 Amplification

In many cases, the signal generated by the primary electrons is not intense enough to be detected by the read-out electronics. Consequently, the charge of the secondary electron cloud must be augmented.

4.8.1 Electron multiplication of the gas

The primary charge generated by ionizing radiation in the gas volume is collected on electrodes by means of an electric field that attracts the the electrons towards the anode and the ions towards the cathode. But the number of primary electrons, generated is too small to be detected by the electronics and so has to be increased in the gas by electron multiplication. At a given gas pressure, the condition is determined

mainly by the gas composition and the electric field strength.

- *Ionisation by electrons:-*

During the migration of these charges, many collisions normally occur with neutral gas molecules. Because of their low mobility, positive or negative ions achieve very little average energy between collisions. Free electrons, on the other hand, are easily accelerated by the applied field and may have significant kinetic energy when undergoing such a collision. If this energy is greater than the ionization energy of neutral gas molecule, it is possible for an additional ion pairs to be created in the collision. Because the average energy of the electron between collisions increases with increasing electric field, there is a threshold value of the field above which this secondary ionization will occur. In typical gases, at atmospheric pressure, the threshold field is of the order of 10^6 V/m. The electrons liberated by this secondary ionization process will also be accelerated by the electric field and in turn can cause further ionization. The number of electrons hence grows with time until all electrons are collected at the anode. This process is known as electron avalanche. At a given field the mean energy of the avalanche electrons is higher in hot gases than in cold gases. It would hence be expected that the largest gains are obtained in noble gases. This is not true in practice because the multiplication process in these gases are not stable.

- *The role of the photons:-*

The cross section for ionization and excitation have roughly the same order of magnitude at electron energies beyond the inelastic thresholds. Therefore, a

comparable number of ionization and excitation occur. In noble gases, the excited states return to the ground state via the emission of photons. Because excitation mainly concerns outer shell electrons, a direct transition to the ground state results in the emission of a photon with an energy in the U V range. De-excitation sometimes involves more than one transition and the energies of the emitted photons are lower in the IR region. Oppositely, molecular gases have several excitation levels with non-radiative relaxation modes. They have a tendency to break into lighter fragments under impact of energetic electrons. IR photons are not sufficiently energetic to impact on the avalanche development. But the UV photons can release new electrons from the gas molecules or from the detector electrodes by the photoelectric effect. The new electrons initiate secondary avalanches, leading to detector instability and eventually to detector breakdown. This process are called photon feedback. It is desirable to stop them early. Molecular gases having absorption bands in the UV range are suited for this task. They are generally mixed with noble gases to stabilize the avalanche process.

- *Penning effect :-*

Penning effect is the ionization of a gas Y by an excited state of a gas X^* . It has two sources. The first one is when an excited atom (Y^*) de-excites by emitting a photon, which is energetic enough to ionize further atom (Y), which have a lower ionization energy as the energy carried by the photon. The second source is when the excited atom has meta-stable states. In this case it cannot emit a photon. The de-excitation occurs through a collision with a second atom resulting in the ionization of the later. Beside increasing the primary ionization

yield, the Penning effect enhances also the gas gain. The multiplication factor can not be increased at will. An empirical limit on the maximum charge that can be tolerated in the avalanche before breakdown was formulated by Raether and corresponds to an avalanche size of approximately 10^8 electrons.

4.8.2 The first Townsend coefficient

The first Townsend coefficient (α) is a term used in an ionization process where there is a possibility of secondary ionization because the primary ionization electrons gain sufficient energy from the accelerating electric field or from the original ionizing particle. The coefficient gives the probability of secondary ionization per unit path length. It is equal to the reciprocal of the mean free path of primary electrons. We can write the average increase of electrons (dN) over a path dS to be

$$dN = N\alpha dS \tag{4.36}$$

The Townsend coefficient α is determined by the excitation and ionization cross section of the electrons that have acquired sufficient energy in the field. It depends on the various transfer mechanism. It also depends on the electric field \vec{E} and increases with the field because the ionization cross section goes up from the threshold as the collision energy increases. It also depends on the gas density linearly.

Theoretical consideration of gas amplification [7] in proportional counter has indicated that the ratio of the first Townsend coefficient to the gas pressure, can be generally expressed in the form,

$$\frac{\alpha}{p} = k_a S^m \exp\left(\frac{-L}{S^{1-m}}\right) \tag{4.37}$$

where $S = \frac{E}{p}$ is the ratio of the electric field strength to the gas pressure, and k_a, L, m ($0 < m < 1$) are constant characteristic of the gas. When $m = 0$, the $\frac{\alpha}{p}$ p

formula reduces to the analytical form used by William and Sara (derived from the models on the behavior of electrons in an electric field) and when $m = 1$ it reduces to that assumed by Diethorn (derived by assuming analytical forms for $\frac{\alpha}{p}$). The coefficient α as given by William and Sara is

$$\alpha = pAe^{\frac{-Bp}{E}} \quad (4.38)$$

At high electric field values, the Townsend coefficient saturates because its value approaches the mean free path given by inelastic collision cross section which is constant. In the eq-4.38 A and B are constant which depends on the basic gas composition.

The amplification factor is given by

$$G = \frac{N}{N_0} = \exp\left(\int_{S_{min}}^S \alpha(E(x)) dx\right) \quad (4.39)$$

In case of uniform field, the above equation becomes,

$$G = e^{\alpha\Delta x} \quad (4.40)$$

4.8.3 The Second Townsend Coefficient

At high field collisions of electrons with atoms or molecules can cause not only ionisation but also excitation. De-excitation is often followed by photon emission. The previous considerations are only true as long as photons produced in the course of the avalanche development are of no importance. These photons, however, will produce further electrons by the photoelectric effect in the gas or at the counter wall, which affect the avalanche development. Apart from gas-amplified primary electrons, secondary avalanches initiated by the photoelectric processes must also be taken into account.

$$\beta = \frac{\text{No. of photoelectric effect events}}{\text{No. of avalanche electrons}} \quad (4.41)$$

So the gas gain including photoeffect :

$$G_\beta = G + G(G_\beta) + G(G_\beta)^2 + G(G_\beta)^3 + \dots = \sum_{k=0}^{\infty} G^{k+1} \beta^k = \frac{G}{1 - \beta G} \quad (4.42)$$

Here βG means the average number of electrons released by photons produced in the first avalanches. In the above equation the first term means no photo effect has occurred, the second term means one photo effects has occurred and so on. The last equality holds when $\beta \ll 1$. When $\beta G \rightarrow 1$, continuous discharge independent of primary ionization has occurred. To prevent this quench gas to absorb UV -photons are added.

4.9 Electron loss

During the transport of the electrons two main processes decrease the number of primary electrons. 1) Recombination, 2) Attachment

4.9.1 Recombination

The recombination is the capture of a free electron by a positive ion followed by a photon emission. For molecular ions, a similar recombination reaction occurs. When there is no electric field, ion electron pairs will generally recombine under the force of their electric attraction, emitting a photon in the process. The recombination rate is proportional to the ions and electron densities.

$$\frac{dn}{dt} = -bn_e(t)n_i(t) \quad (4.43)$$

Here n_e is the electron density, n_i is the ion density, b is the recombination coefficient.

If we set $n_e = n_i = n$ then integration yields

$$\begin{aligned} \frac{dn}{dt} &= -bn^2 \\ \Rightarrow \int_{n_0}^n \frac{dn}{n^2} &= -b \int_0^t dt \\ \Rightarrow \left[-\frac{1}{n} \right]_{n_0}^n &= -bt \\ \Rightarrow \frac{1}{n} &= \frac{1}{n_0} - bt \end{aligned}$$

So we have

$$n = \frac{n_0}{1 + bn_0t} \tag{4.44}$$

here n_0 is the initial concentration at $t = 0$.

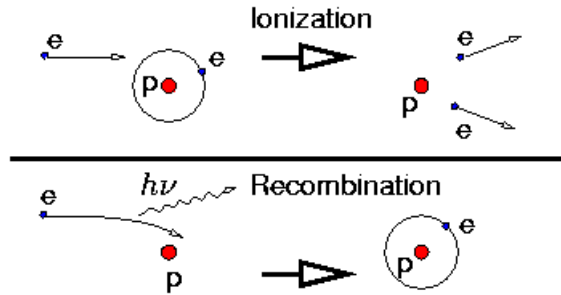


Figure 4.2: Process of recombination and Ionisation.

4.9.2 Electron Attachment

During their drift, electrons may be absorbed in the gas by the formation of negative ions. Whereas the noble gases and most organic molecules can form only stable negative ions at collision energies of several electron volts (which is higher than the energies reached during the drift in gas chambers), there are some molecules that are capable of attaching electrons at much lower collision energies. Such molecules are sometimes present in the chamber gas as impurities. Among all the elements, the

largest electron affinities, i.e. binding energies of an electron to the atom in question, are found with the halogenides ($3.13.7eV$) and with oxygen ($\sim 0.5eV$). Therefore we have in mind contaminations due to air, water, and halogen-containing chemicals. The break-up of the molecule owing to the attaching electron is quite common and is called dissociative attachment. The probability of the molecule staying intact is generally higher at lower electron energies. The rate R of attachment is given by the cross-section σ , the electron velocity c , and the density N of the attaching molecule:

$$R = c\sigma N \tag{4.45}$$

Chapter 5

Measurement of Ionization

The moving charges in a chamber give rise to electrical signals on the electrodes that can be read out by amplifiers. The electrons created in the avalanche close to the wire move to the wire surface within a time typically much less than a nanosecond, resulting in a short signal pulse. The ions created in the avalanche move away from the wire with a velocity about a factor 1000 smaller, which results in a signal with a long tail of typically several hundred microseconds duration. The movement of these charges induces a signal not only on the wire but also on the other electrodes in the chamber, so for the purpose of coordinate measurements the cathode can be subdivided into several parts. In this chapter we derive very general theorems that allow the calculation of signals in wire chambers and present some practical examples.

5.1 Signals Induced on Grounded Electrodes, Ramos Theorem

Contrary to what might be inferred from the brief description of ionization detectors, the pulse signal on the electrodes of ionization devices is formed by induction due to the movement of the ions and electrons as they drift towards the cathode and anode, rather than by the actual collection of the charges itself. A method of computing the induced current for a charge motion is explained here with the derivation of the formula using basic electrodynamic identities.

Consider a charge (q), in the presence of any number of grounded conductors, for one of any number of grounded conductors, for one of round the electron with a

tiny equipotential sphere. Then if V is the potential of the electrostatic field, in the region between conductors

$$\nabla^2 V = 0 \quad (5.1)$$

where ∇^2 is the Laplacian operator. Call V_q the potential of the tiny sphere and note that $V = 0$ on the conductors and

$$-\oint_S \frac{\partial V}{\partial n} ds = q/\epsilon_0 (\text{Gauss' law}) \quad (5.2)$$

Where the integral is done over a surface of the sphere and $\partial V/\partial n$ indicates differentiation with respect to the outward normal to the surface and the integral is taken over the surface of the sphere. Now consider the same set of conductors with the electron removed, conductor A raised to unit potential and the other conductors grounded. Call the potential of the field in this case V' , so that $\nabla^2 V' = 0$ in the space between conductors, including the point where the electron was situated before. Call the new potential of this point V'_q . Now Green's theorem states that

$$\oint_B [V' \nabla^2 V - V \nabla^2 V'] dv = - \oint_B \left[V' \frac{\partial V}{\partial n} - V \frac{\partial V'}{\partial n} \right] ds \quad (5.3)$$

Here B represents the boundary and ds means that is a surface integral over the boundary and dv means a volume integral. S stands for the sphere and A is the region of chosen conductor on which we are calculating the induced charge.

Choose the volume to be that bounded by the conductors and the tiny sphere. Then the left-hand side is zero and the right-hand side may be divided into three integrals:

- (1) Over the surfaces of all conductors except A. This integral is zero since $V = V' = 0$ on these surfaces.
- (2) Over the surface of A. This reduces to $-\oint_A \frac{\partial V}{\partial n} ds$ for $V' = 1$ and $V = 0$ for conductor A.

(3) Over the surface of the sphere. This becomes $-V'_q \oint_S \frac{\partial V}{\partial n} ds + V_q \oint_S \frac{\partial V'}{\partial n} ds$

The second of these integrals is zero by Gauss' law since $\int (\partial V' / \partial n) ds$ is the negative of the charge enclosed (which was zero for the second case in which the electron was removed). Finally, we obtain from (2)

$$0 = - \oint_A \frac{\partial V}{\partial n} ds + V'_q \oint_S \frac{\partial V}{\partial n} ds = Q_A / \epsilon_0 - q V'_q / \epsilon_0 \quad (5.4)$$

$$\Rightarrow Q_A = q V'_q$$

Now taking the derivative w.r.t. time we get the induced current;

$$i_A = \frac{dQ_A}{dt} = q \frac{dV'_q}{dt} = q \left[\frac{\partial V'_q}{\partial x} \frac{dx}{dt} \right] \quad (5.5)$$

where x is the direction of the motion.

Now $\frac{dx}{dt} = v$ and $\frac{\partial V'_q}{\partial x} = -E_v$, where E_v is electric field parallel to velocity of charge.

so we have,

$$i = -qvE_v \quad (5.6)$$

5.2 Induced Signals in a Drift Tube

For the cylindrical proportional counter, Fig-5.2 the electric field and potential can be written as

$$E(r) = \frac{CV_0}{2\pi\epsilon r} \quad (5.7)$$

$$\phi(r) = -\frac{CV_0}{2\pi\epsilon} \ln(r/a) \quad (5.8)$$

where r is the radial distance from the wire, V_0 the applied voltage, ϵ the dielectric constant of the gas, and

$$C = \frac{2\pi\epsilon}{\ln(b/a)} \quad (5.9)$$

is the capacitance per unit length of this configuration.

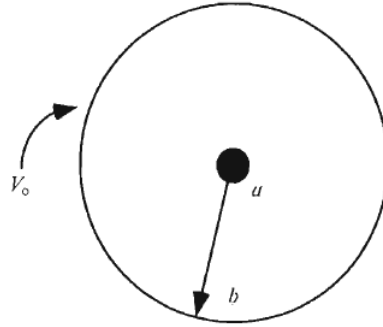


Figure 5.1: Cylindrical proportional tube with outer radius b at voltage V_0 and inner (wire) of radius a at voltage zero.

Suppose that there is now a charge q located at a distance r from the central wire. The potential energy of the charge is then the potential energy is $W = q\phi(r)$. If now the charge moves a distance dr , the change in potential energy is

$$dW = q \frac{d\phi(r)}{dr} dr \quad (5.10)$$

For a cylindrical capacitor, however, the electrostatic energy contained in the electric field is $W = \frac{l}{2}CV^2$, where l is the length of the cylinder. If the movement of the charges is fast relative to the time that an external power supply can react to changes in the energy of the system, we can consider the system as closed. Energy is then conserved, so that

$$dW = lCV_0dV = q \frac{d\phi(r)}{dr} dr \quad (5.11)$$

Thus there is a voltage change,

$$dV = \frac{q}{lCV_0} \frac{d\phi(r)}{dr} dr \quad (5.12)$$

induced across the electrodes by the displacement of the charge. Eq.-5.12 is a general result, in fact, and can be used for any configuration.

or our cylindrical proportional counter, let us assume that an ionizing event has occurred and that multiplication takes place at a distance r' from the anode. The total induced voltage from the electrons is then

$$V^- = \frac{-q}{lcV_0} \int_{a+r'}^a \frac{d\phi}{dr} dr = -\frac{q}{2\pi\epsilon l} \ln \left(\frac{a+r'}{a} \right) \quad (5.13)$$

while that from the positive ions is

$$V^+ = \frac{q}{lcV_0} \int_{a+r'}^b \frac{d\phi}{dr} dr = -\frac{q}{2\pi\epsilon l} \ln \left(\frac{b}{a+r'} \right) \quad (5.14)$$

The sum of the two contributions is then $V = V^- + V^+ = -q/lC$ and the ratio of their contributions is

$$\frac{V^-}{V^+} = \frac{\ln \frac{a+r'}{a}}{\ln \frac{b}{a+r'}} \quad (5.15)$$

Since the multiplication region is limited to a distance of a few wire radii, it is easy to see that the contribution of the electrons is small compared to the positive ions. Taking some typical values of $a = 10\mu m$, $b = 10mm$ and $r' = 1\mu m$, V^- turns out to be less than 1% of V^+ . The induced signal, therefore, is almost entirely due to the motion of the positive charges and one can ignore the motion of the electrons. With this simplification we can now calculate the time development of the pulse. Thus,

$$V(t) = \int_{r(0)}^{r(t)} \frac{dV}{dr} dr = -\frac{q}{2\pi\epsilon l} \ln \frac{r(t)}{a} \quad (5.16)$$

To find $r(t)$, considering the mobility to be constant;

$$\frac{dr}{dt} = \mu E(r) = \frac{\mu CV_0}{2\pi\epsilon} \ln \frac{r(t)}{a} \quad (5.17)$$

solving the differential equation we get;

$$r(t) = \left(a^2 + \frac{\mu CV_0}{\pi\epsilon} t \right)^{1/2} \quad (5.18)$$

Now using this expression for the $r(t)$ we can calculate the induced voltage and the induced charge just by multiplying the capacitance and the time derivative of that

will give us the induced current. The wire signal is negative and has a hyperbolic form with a characteristic time constant t_0 , which in practical cases will be a few nanoseconds. The induced current at time t is given by

$$I(t) = \frac{dQ(t)}{dt} = Cl \frac{dV(t)}{dt} = \frac{-q}{2\ln(b/a)} \frac{d}{dt} \left[\ln \left(1 + \frac{t}{t_0} \right) \right] \quad (5.19)$$

$$\Rightarrow I(t) = \frac{-q}{2\ln(b/a)} \frac{1}{t + t_0}$$

where $t_0 = a^2\pi\epsilon/\mu CV_0$.

We could have calculated this easily by using Ramo's theorem. First calculate $r(t)$ then the derivative will give the velocity and then multiplying with the electric field we will get the induced current per unit charge.

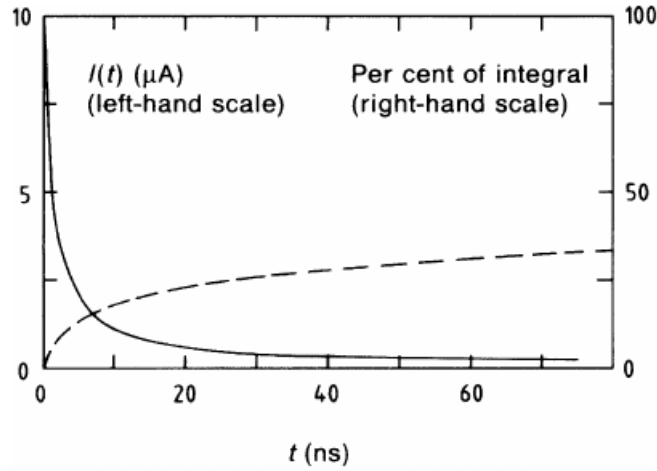


Figure 5.2: Current signal according to Eq-5.19 (full line, left-hand scale) for $t_0 = 1.25ns$, $b/a = 500$, and $q = 10^6 * e$. Time integral of this pulse (Induced charge) as a percentage of the total (broken line, right-hand scale)

Since the electric field in the vicinity of the wire of any wire chamber has the form $1/r$, the universal shape of the induced current signal $I(t)$ Eq.-5.19 is valid for wire signals of all wire chamber geometries.

Chapter 6

Simulation of Gaseous detectors

Few definitions to start with:

Model: A system of postulates, data and interfaces presented as a mathematical description of an entity or proceedings or state of affair. (Development of equations, constraints and logic rules.)

Simulation: Exercising the model and obtaining results. (Implementation of the model). Simulation has emerged as the Third methodology of exploring the truth. It would complement the theory and experimental methodology. Simulation will never replace them. There are many tangible benefits like Saves manpower, material ; useful even if not possible by other means; saves money with fast, consistent answers ; could be used for education after establishing and intangible benefits like increased flexibility, accuracy, range of operation ; new results not available before ; improved results due to standardisation ; increased understanding ; explicitly stated assumptions and constraints in simulations.

The major investments are computer,skill/experties, time for implementation. There are pitfalls too,

- Modelling errors at different levels -Scientific model of reality, Mathematical model, discrete numerical model, application program model, computational model
- Input errors: Out of range inputs can give spurious results
- Precision errors: Limits in the precision

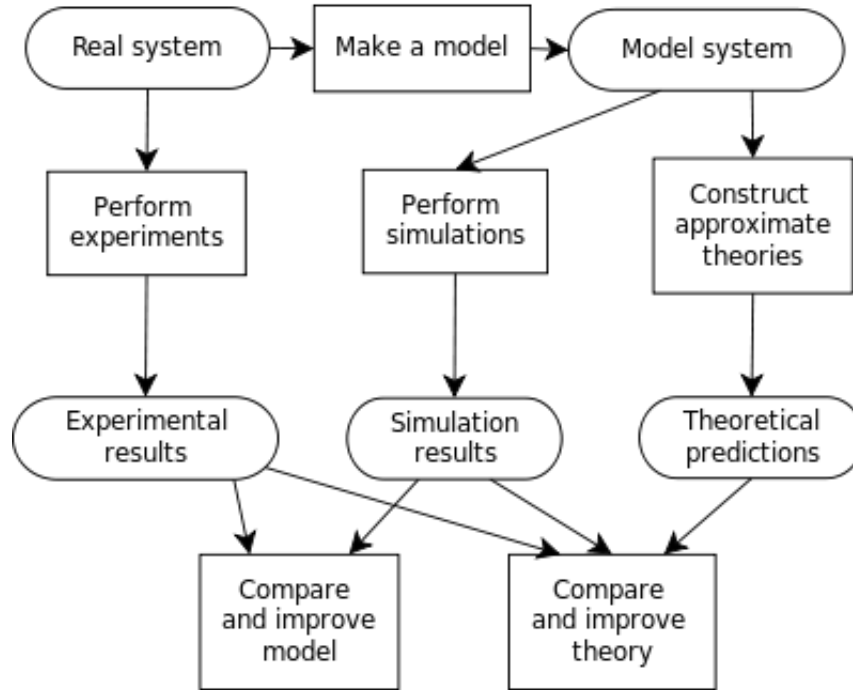


Figure 6.1: An overview of the different methods on quest of truth is explained through a flow chart

6.1 Simulation tools

We are trying to simulate different gaseous detectors using software packages like GARFIELD, neBEM, MAGBOLTZ.

- **GARFIELD** : Detector Modelling (specifying the geometry) , Detector Response (charge induction using Reciprocity theorem, particle drift, charge sharing, charge collection)
- **neBEM** : (nearly exact Boundary Element Method)
Electrical Solver: charge distribution on a geometry for a given voltage configuration; both potential and field computed using the charge distribution
- **MAGBOLTZ** : Transport and Amplification
electron drift velocity and diffusion coefficients (longitudinal and transverse),

Townsend and attachment coefficients

6.1.1 Garfield

Garfield, developed by R. Veenhof [12], is a widely used program for detailed simulation of two and three dimensional drift chambers. The software uses field maps for these drift chambers as the basis for its calculations. After that, particle drift including diffusion, avalanches and finally the signal on the read-out electrode can be calculated.

Garfield provides an efficient two and three dimensional geometry modeler. Different two dimensional (such as infinite equipotential plane, tube) and three dimensional (such as box with right angles, box with a cylindrical hole in center, cylinder, thin-wire, sphere etc.) elements are defined inside the software. A specific detector geometry can be modelled with the help of these elements. The description of the specified chamber can either be in polar or in Cartesian coordinates and consists of a listing of the position, dimension and potential or dielectric constant.

Garfield has its own library to analytically calculate the electric field when the detector geometry can be decomposed in equipotential planes, wires and tubes without intersections. For more complicated geometries, the program provides interfaces with different field solvers.

Considering only the electrostatic fields, the trajectory of an electron or ion would be such that the position as a function of the time, $\vec{r}(t)$, should obey the following differential equation

$$m_e \frac{d^2 \vec{r}(t)}{dt^2} = e \vec{E}(\vec{r}(t)) \quad (6.1)$$

where m_e and e are the mass and the electric charge of the electron. In order to

correctly simulate the drift of the electrons in real gases, Garfield has other integration methods which employs Monte Carlo calculation that takes diffusion into account.

Finally, Garfield simulates the signal induced on the read-out electrodes resulting from the passage of a charged particle through the chamber. The electron pulse is computed by following the avalanche process along the electron drift line. The current induced by the avalanche ions is also computed according to a simplified model.

6.1.2 MAGBOLTZ

Magboltz was developed by S. Biagi [13] to calculate the transport parameters of electrons drifting in the gases under the influence of electric and magnetic field. The program computes electron transport parameters by numerically integrating the Boltzmann transport equation. By tracking the electron propagation, the program can compute the drift velocity, the longitudinal and transverse diffusion coefficients and Townsend and attachment coefficients in various gases. By including a magnetic field, it can also calculate the Lorentz angle. The collision types involve elastic and inelastic collisions, attachment, ionization and super-elastic collisions. The collision angular distributions have also been introduced. The program contains, for 60 gases, electron cross-sections for all relevant interactions with atoms and/ or molecules. The gas descriptions are still being improved. In order to improve the simulation and also maintain the desired accuracy, the Monte Carlo integration technique has been applied to the solution of the transport equations in the more recent versions of the code.

- Results using MAGBOLTZ

The theory on transport properties of charges in gases are used with the help of Monte-Carlo method in MAGBOLTZ. Here some of the gas properties are plotted against the electric field and the variations are observed which verifies the above

mentioned equations.

Variation of drift velocity in different gas mixtures like Argon- CO_2 in different volume ratios 70-30 , 90-10 and Neon- CO_2 in 90-10 and Neon- $CO_2 - N_2$ in volume ratio of 90-10-5 are taken into consideration.

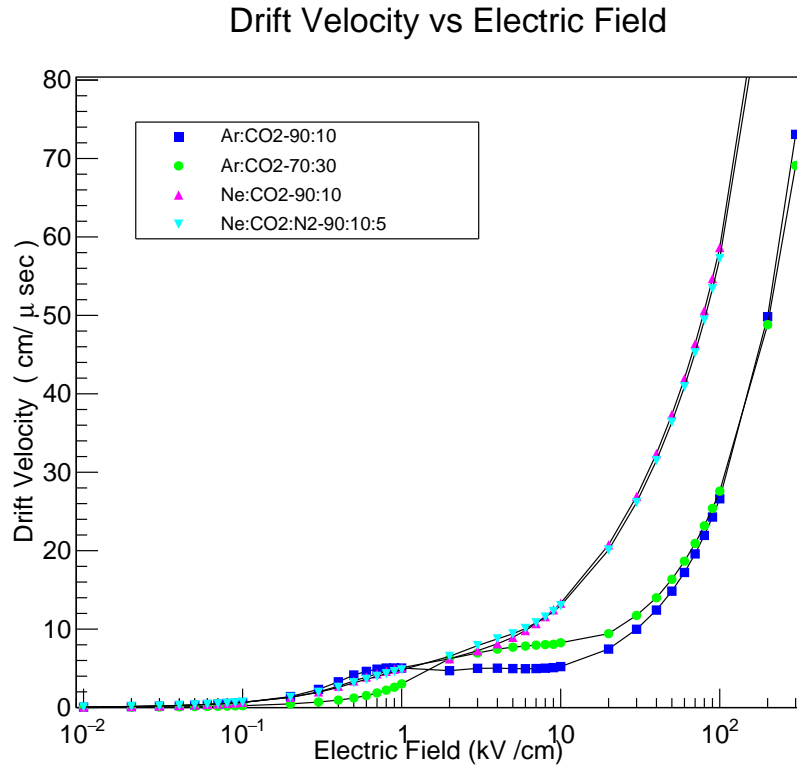


Figure 6.2: Variation of drift velocity of electron in different gas mixtures.

The pairing of lines are completely showing that it is much more dependent on the base gas like Ar or Ne and the slight difference is due to the change in quenching gas. Attachment coefficient and Townsend coefficient are plotted which depends on the in-elastic scattering cross-section of the gases used in the magboltz.

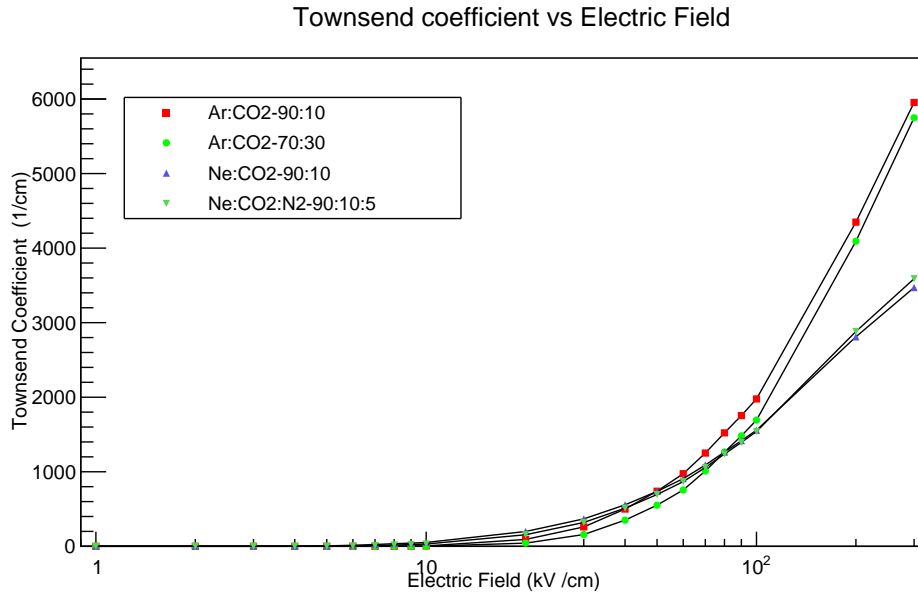


Figure 6.3: Variation of Townsend coefficient of electron in different gas mixtures.

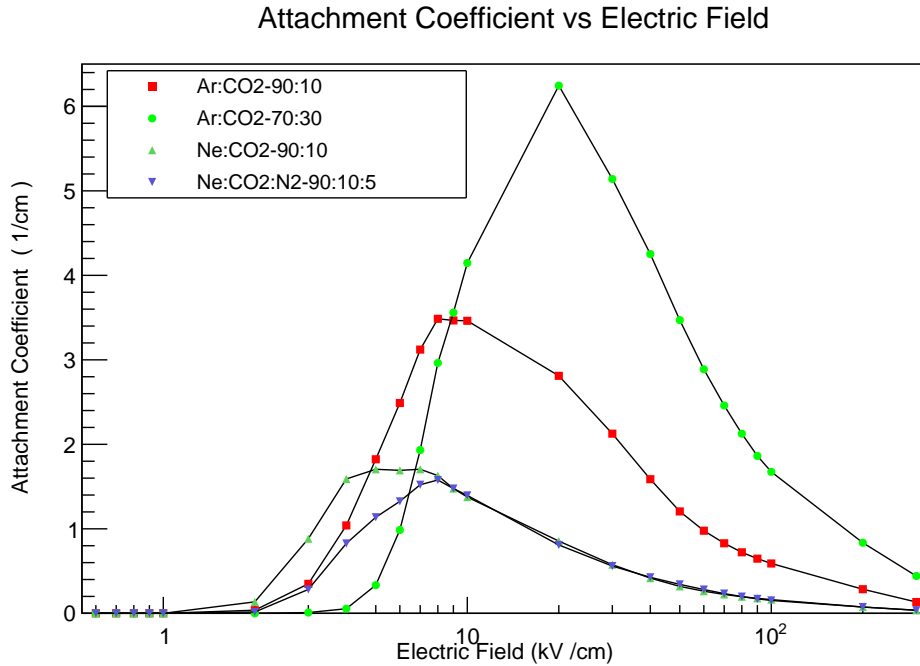


Figure 6.4: Variation of attachment coefficient of electron in different gas mixtures.

The variation of longitudinal and transverse diffusion coefficient are given below.

The pairing of lines at high electric field value is clear and diffusion coefficients are same for all low electric field values.

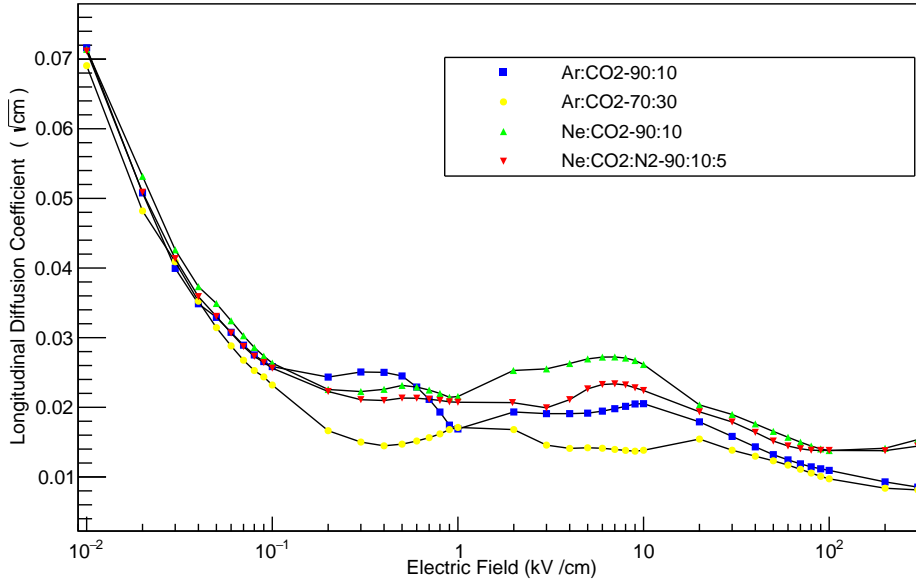


Figure 6.5: Variation of longitudinal diffusion coefficient of electron in different gas mixtures.

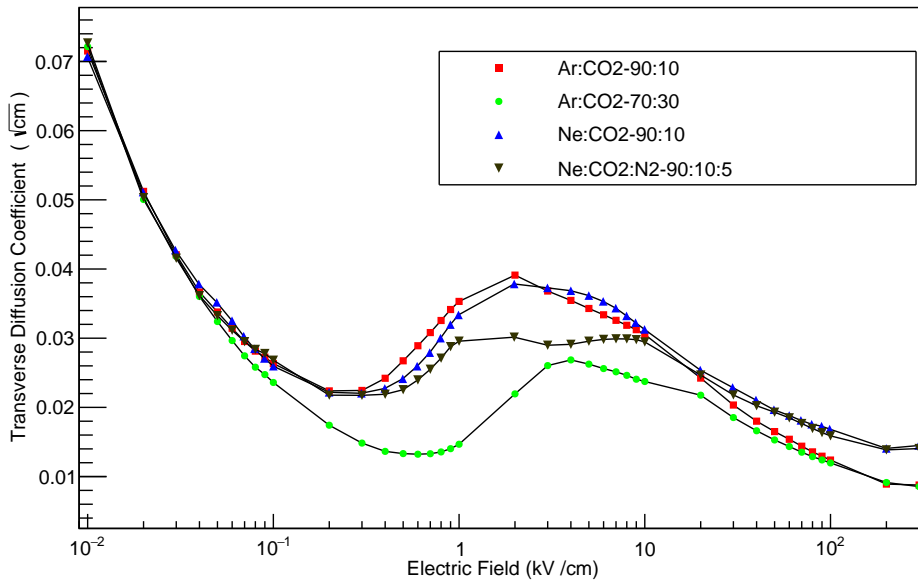


Figure 6.6: Variation of Transverse diffusion coefficient of electron in different gas mixtures.

For the variation with the magnetic field values we have taken $Ne-CO_2-N_2$ (90-10-5) and except for the diffusion coefficient there was no variation in any other parameters. The variation in transverse diffusion coefficient is clear from the eq-4.34 & 4.35.

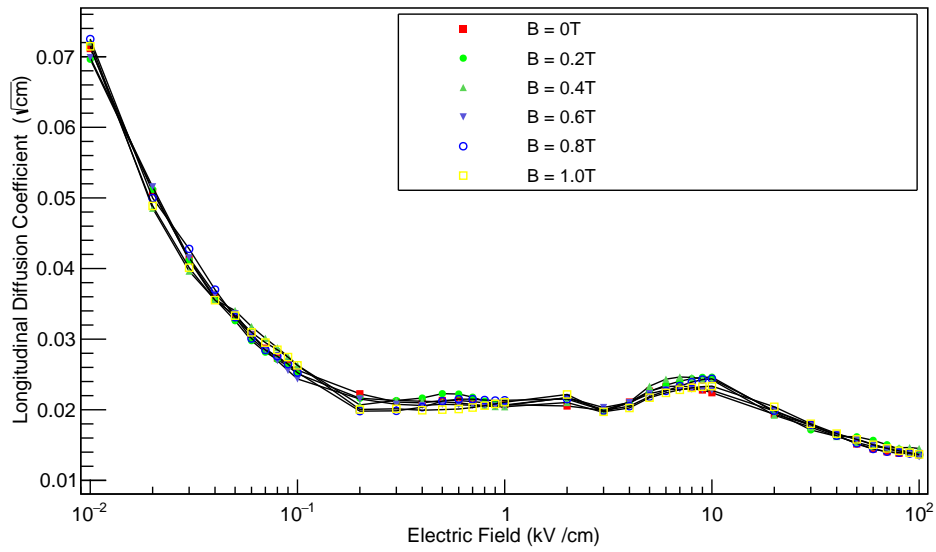


Figure 6.7: Variation of longitudinal diffusion coefficient of electron in $Ne-CO_2-N_2$ (90-10-5) with magnetic field.

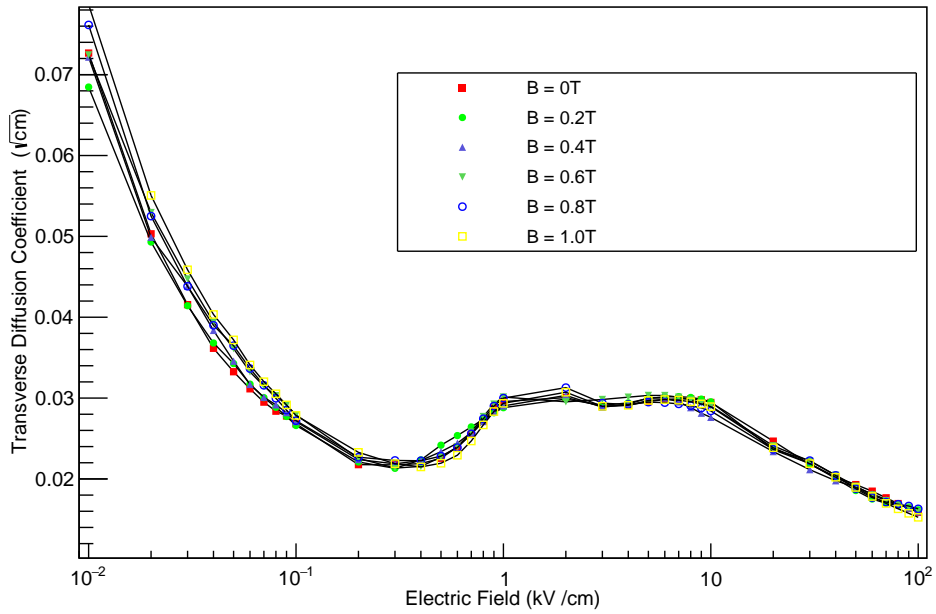


Figure 6.9: Variation of transverse diffusion coefficient of electron in $\text{Ne-CO}_2\text{-N}_2$ (90-10-5) with magnetic field (Perpendicular to electric field).

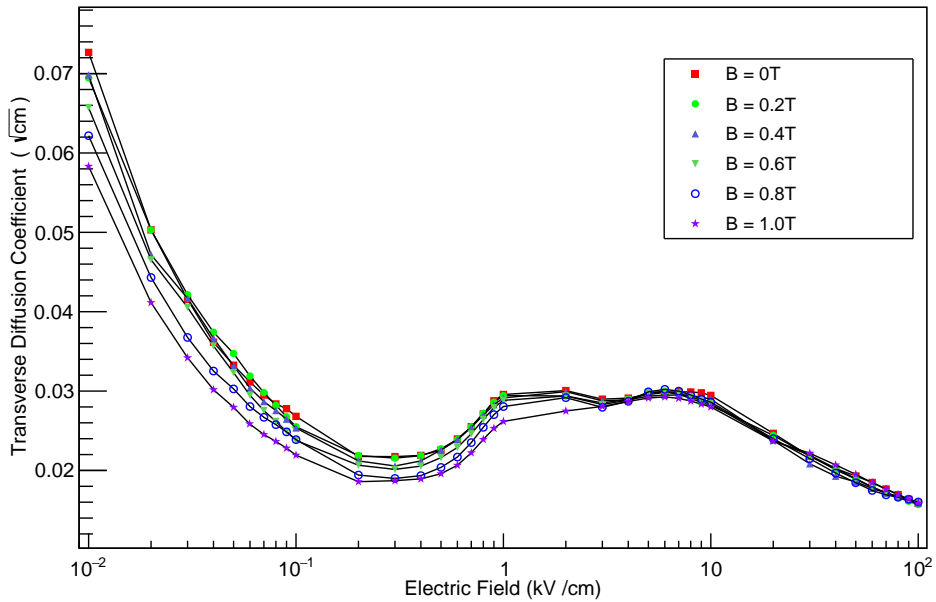


Figure 6.8: Variation of transverse diffusion coefficient of electron in $\text{Ne-CO}_2\text{-N}_2$ (90-10-5) with magnetic field (parallel to electric field).

The spreading in the low electric field values for the transverse diffusion coefficient

is more when the electric field and magnetic field are parallel and less when they are perpendicular to each other. (As the Lorentz force is perpendicular to the Magnetic field applied).

6.1.3 Calculation of the electric field

The process of detailed detector simulation begins with computing estimates of the electromagnetic field configuration of a given device under experimental conditions. The efficiency and precision of the field solver determines a large number of parameters and processes that finally determine the detector characteristics and performance. For example, the field configuration is a key factor in determining the amount of ionization and multiplication in a gas. In addition, non-linear effects of space charge, dynamic charging processes within ionization detectors makes fast but reliable estimation of electromagnetic fields, a must. While the importance of correctly estimating the field configuration has always been of major importance in understanding a gas ionization detector, it is found to be even more difficult and demanding for micro-pattern gas detectors. This is so because of the large variation in length scales, presence of very closely spaced surfaces leading to possible degeneracy of boundary conditions, the importance of resolving various properties and processes to smaller scales, possibility of unwanted and damaging sparks or discharges and intricate small patterns leading to large variation in potential and flux within very small distances. The problem is further complicated through the existence multiple dielectrics in a given device.

The BEM [5], Boundary Element Method , solves the problem only at the boundary elements. If an arbitrary point of interest does not match with a nodal point of a finite- difference or finite-element mesh, property values at the surrounding mesh needs to be inter / extrapolated resulting in an obvious loss of accuracy. Since this method solves for potential and uses low-order polynomials to represent it, the electric

field values are found to be even 50% in error in regions where the fields values are changing rapidly, e.g., near an anode wire in a proportional counter. It may be noted here that since a charged particle in a gas detector can occur at any point within the detector and cause an avalanche, accurate knowledge of electric field at any arbitrary point within a detector is crucially important to be able to track the behavior of the charged particle and the avalanche.

Poissons equation for electrostatic potential

$$\nabla^2\phi = -\rho/\epsilon_0 \quad (6.2)$$

can be solved to obtain the distribution of charges which leads to a given potential configuration ϕ . Here ρ is the charge density and ϵ_0 is the permittivity of free space. For a point charge q at \vec{r}' in 3D space, the potential $\phi(\vec{r})$ at \vec{r} is known to be

$$\phi(\vec{r}) = \frac{q}{4\pi\epsilon_0|\vec{r} - \vec{r}'|} \quad (6.3)$$

For a general charge distribution with charge density $\rho(\vec{r}')$, superposition holds and results in

$$\phi(\vec{r}) = \int \frac{\rho(\vec{r}')dv'}{4\pi\epsilon_0|\vec{r} - \vec{r}'|} = \int G(\vec{r}, \vec{r}')\rho(\vec{r}')dv' \quad (6.4)$$

where

$$G(\vec{r}, \vec{r}') = \frac{1}{4\pi\epsilon_0|\vec{r} - \vec{r}'|} \quad (6.5)$$

is the free space Greens function for the Laplace operator in 3D. Similarly, the field for a general charge distribution can be written as

$$\vec{E}(\vec{r}) = -\nabla\phi \quad (6.6)$$

so we have

$$\vec{E}(\vec{r}) = -\nabla \left(\int G(\vec{r}, \vec{r}')\rho(\vec{r}')dv' \right) \quad (6.7)$$

and, finally

$$\vec{E}(\vec{r}) = \int \frac{\rho(\vec{r}')(\vec{r} - \vec{r}')dv'}{4\pi\epsilon_0|\vec{r} - \vec{r}'|^3} \quad (6.8)$$

The charge distribution can be obtained from equation (4.3) or (4.7) by satisfying the boundary conditions at collocation points known either in the form of potential (Dirichlet) or field (Neumann) or a mixture of these two (Mixed/Robin) on material boundaries/surfaces present in the domain. Considering the Dirichlet problem only at present (for ease of discussion), the following integral equation of the first kind can be set up.

$$\phi(\vec{r}) = \int_{vol} G(\vec{r}, \vec{r}')\rho(\vec{r}')dv' \quad (6.9)$$

Here, $\phi(\vec{r})$ is the potential at a point \vec{r} in space and $\rho(\vec{r}')$ is the charge density at an infinitesimally small volume dv' placed at \vec{r}' . The problem is, generally, to find $\rho(\vec{r}')$ as a function of space resulting the known distribution of $\phi(\vec{r})$. Once the charge distribution on the boundaries and all the surfaces are known, potential and field at any point in the computational domain can be obtained using the same equation (4.8) and its derivative.

The primary step of the BEM technique is to discretize the boundaries and surfaces of a given problem. The elements resulting out of the discretization process are normally rectangular or triangular though elements of other shapes are also used. In the collocation approach, the next step is to find out charge distribution on the elements that satisfies equation (4.8) following the given boundary conditions. The charge distribution is normally represented in terms of known basis functions with unknown coefficients. For example, in zeroth order formulations using constant basis function, which is also the most popular one among all the BEM formulations because of a good optimization between accuracy and computational complexity, the charge distribution on each element is assumed to be uniform and equivalent to a point

charge located at the centroid of the element.

Since the potentials on the surface elements are known from the given potential configuration, equation (3) can be used to generate algebraic expressions relating unknown charge densities and potentials at the centroid of the elements. One unique equation can be obtained for each centroid considering influences of all other elements including self influence and, thus, the same number of equations can be generated as there are unknowns. In matrix form, the resulting system of simultaneous linear algebraic set of equations can be written as follows

$$\mathbf{K} \cdot \rho = \phi \quad (6.10)$$

where \mathbf{K} is the matrix consisting of influences among the elements due to unit charge density on each of them, ρ represents a column vector of unknown charge densities at centroids of the elements and ϕ represents known values of potentials at the centroids of these elements. Each element of this influence coefficient or capacity coefficient matrix, \mathbf{K} is a direct evaluation of an equation similar to equations (4.3) or (4.7) which represents the effect of a single element on a boundary/surface (obtained through discretization) on a point where a boundary condition of the given problem is known. While, in general, this should necessitate an integration of the Greens function over the area of the element, this integration is avoided in most of the BEM solvers through the assumption of nodal concentration of singularities with known basis function.

Since the right hand side of (4.9) is known, in principle, it is possible to solve the system of algebraic equations and obtain surface charge density on each of the element used to describe the conducting surfaces of the detector following

$$\rho = \mathbf{K}^{-1} \cdot \phi \quad (6.11)$$

Once the charge density distribution is obtained, equations (4.3) and (4.7) can be used to obtain both potential and field at any point in the computational domain.

The nearly exact prefix refers to a way of addressing the singularities near the boundaries. In the neBEM approach, the integrations for evaluating influences (both potential and flux) due to rectangular and triangular elements having uniform charge density have been obtained as closed-form analytic expressions using symbolic mathematics. The Inverse Square Law Exact Solutions (ISLES) library is a small library of C functions based on the analytic closed-form expressions mentioned before. Since any real geometry can be represented through elements of the above two types (or by the triangular type alone), this library has allowed us to develop the neBEM solver that is capable of solving three-dimensional potential problems involving arbitrary geometry. Its application is not limited by the corners, edges, proximity of other singular surfaces or their curvature or their size and aspect ratio. It may be noted here that any non-right-angled triangle can be easily decomposed into two right-angled triangles. Thus, the right-angled triangles considered here, in fact, can take care of any three-dimensional geometry.

6.1.4 Accuracy check of neBEM

Calculations for electric field value using neBEM and the theoretically calculated value for a particular voltage configuration has been carried out. The electric field value (only magnitude) for a cylindrical proportional chamber comes with an expression

$$E = \frac{V}{r \ln\left(\frac{b}{a}\right)} \quad (6.12)$$

For this simple case it can easily be said that electric field is radially outward from the geometry of the model.

Where $b \rightarrow$ inner radius of the cylinder

a → radius of the central wire

r → radial distance from the axis

V → Potential difference between the electrodes

We have taken a particular configuration with $b = 0.8\text{cm}$, $a = 0.005\text{cm}$ and $V = 2000$ volt. Defining the geometry needs a parameter (say n), which defines the number of sides of the surface of the hole. For example $n=2$ means the cross section of the hole will be a polygon with sides 4 ($4n-4$). So for a perfect circular hole n should be infinity but then it is time consuming to take a high value of n and do the calculation. In order to observe the effect from the value of n a comparison has been taken by two different values of the n and comparing with theoretically calculated values. The table found out to be

r in cm	E_{Theory}	E_{Cal} (n=4)	% error	E_{Cal} (n=10)	% error
0.05	7881.50	7921.84	0.512	7888.19	0.084
0.1	3940.75	3960.8	0.509	3943.95	0.081
0.2	1970.38	1980.16	0.496	1971.7	0.067
0.3	1313.58	1319.86	0.478	1314.18	0.045
0.7	562.97	586.82	4.236	562.75	0.039

Table 6.1: Comparison of theoretical calculation and neBEM field values.

We can see clearly that the error decreases very rapidly by changing value of n from 4 to 10. So a moderate value of n was taken for the rest of the calculations. This shows the accuracy of neBEM with theory.

As an output from Garfield we can get for example the drift lines of the electrons and ions, a visualisation of the electric field which is calculated from the potential, or the number of electrons and ions produced in avalanches. This last value is important

to get values for the gain and the ion-backdrift. The same approach is valid for double and triple GEM stacks with the only difference being that the corresponding basic cell consists of several single GEM basic cells arranged in a stack. The aim of the Garfield-simulation is to obtain values for the gain and the Ion-backdrift and to determine their dependence on different GEM parameters like the GEM voltages or the distances between the GEMs in the stacks.

Chapter 7

Results and Discussion

The general theory of gaseous ionisation detectors have been used in two different cases 1)MWPC and 2) GEM

7.1 Multi Wire Proportional Chamber

In 1968, Georges Charpak, while at the European Organization for Nuclear Research in CERN, invented and developed the multi-wire proportional chamber (MWPC). The chamber was an advancement of the earlier bubble chamber, rate of detection of only one or two particles every second to 1000 particle detections every second. A multiwire proportional chamber (MWPC) consists of a plane of equally spaced anode wires, sandwiched between two cathode planes. The equipotential lines for such a structure show three regions of electric field . In the major part of the volume the field is uniform ; close to the wire it varies inversely with the distance r to the axis, almost exactly as in a cylindrical counter; and just between the wires there is a small region of very low field . If a particle produces ion pairs in the gas of such a structure, the liberated electrons drift towards the anode wire. Reaching its vicinity a multiplicative avalanche develops. We find the same variety of amplification processes : an avalanche size proportional to the number of initial electrons for low gains, an amplification saturated by space-charge effects for high gains, a propagation by secondary photons for gases with low quenching properties leading either to a Geiger type propagation along the wires or or to a streamer mode, interrupted or bridging the electrodes and followed by a spark.

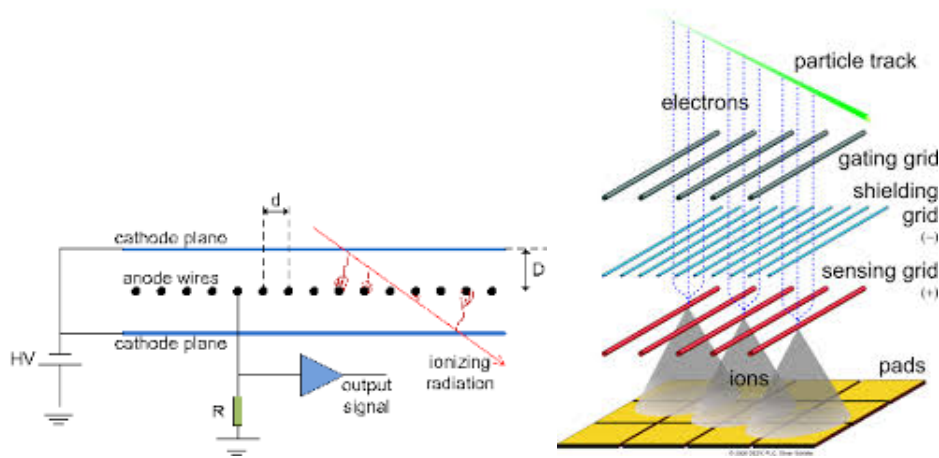


Figure 7.1: Schematic diagram of a MWPC read out and use of gating grid.

In order to get the controls over the charges flowing towards the anode wire a gating grids are placed in between the anode wire and cathode plane. Using the GARFIELD the geometry has been created for a single cell which contains a single wire and later using periodicity it can be expanded to arbitrary number of anode wires later. The voltage configuration and the electric field intensity along the z-axis is plotted.

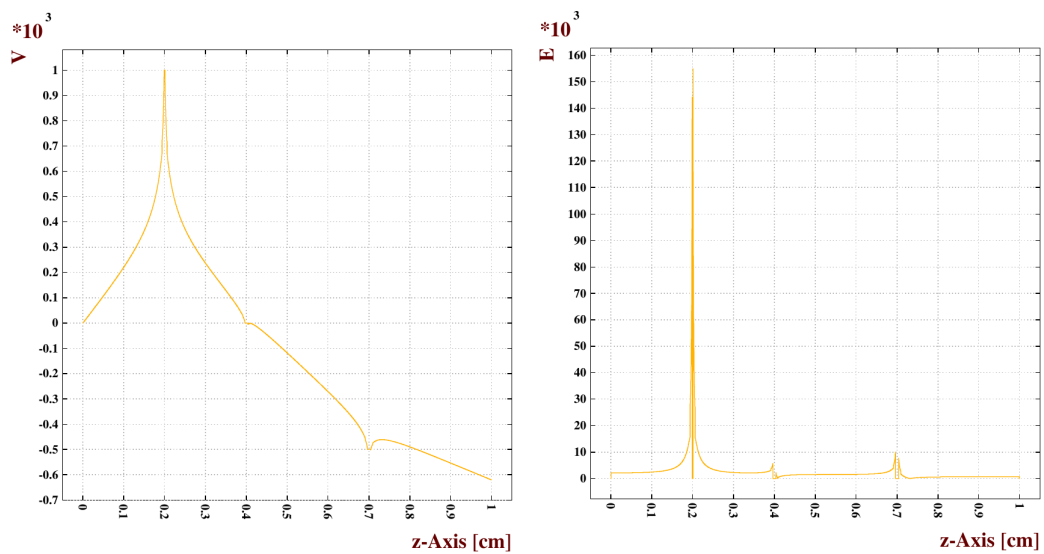


Figure 7.2: Voltage and Electric field configuration of MWPC.

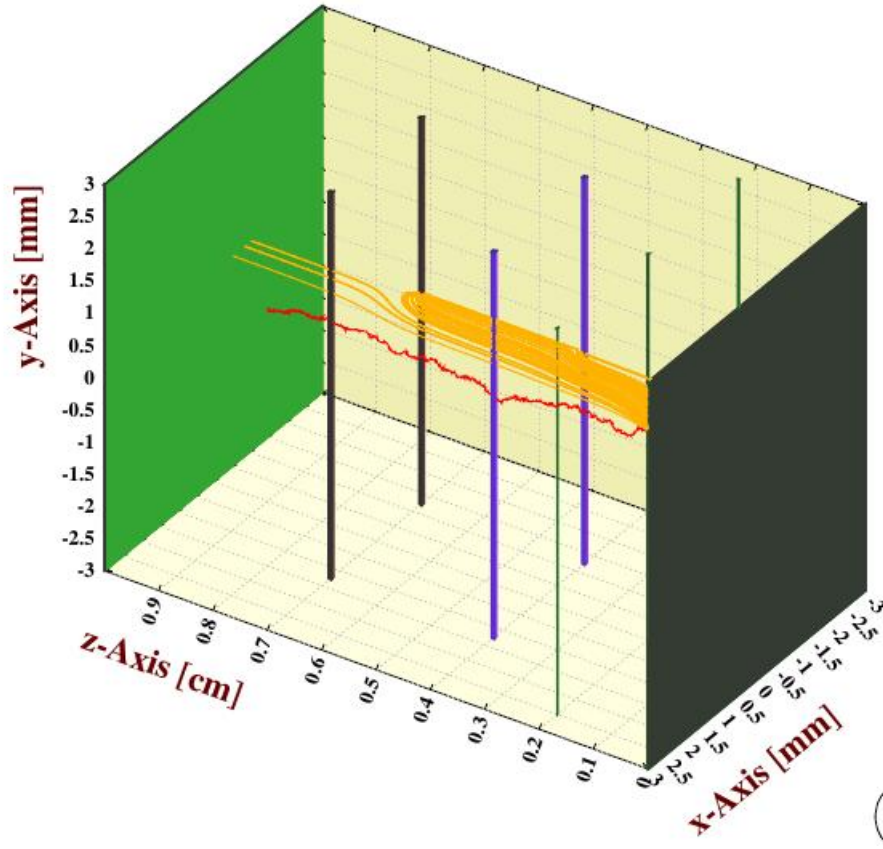


Figure 7.3: Simulating an Avalanche in MWPC.

Electron (red line) is drifting from $(0,0,0.9)$ to $(0,0,0.2)$ near which avalanche is happening and ions (yellow lines) are moving towards the cathode plate. Some of them are getting attached in the gating grid.

7.2 Gas Electron Multiplier

The Gas Electron Multiplier (GEM) detector is another common choice among MPGDs for tracking and triggering in particle physics experiments. In harsh radiation environments of high-luminosity colliders, these detectors offer excellent spatial and temporal resolution. Besides that, the large sensitive area and the operational stability make this detector a promising candidate in different fields. In the present work, numerical simulation has been used as a tool of exploration to evaluate the fundamental features of a single GEM detector.

The Gas Electron Multiplier (GEM) was introduced in 1996 by Sauli [11]. It is a composite grid structure consisting of two metal layers separated by a thin insulator which is etched with a regular matrix of holes (Figure 7.4). Applying a voltage between the two conductive plates, a strong electric field is generated inside the holes (E_{GEM} in Figure 7.7). It separates the gas volume in three regions: a low field drift region above the GEM where the primary charge is produced, a high field region inside the holes where the electrons are multiplied and an induction region below the GEM where about 50% of the avalanche electrons drift to the read-out electrodes.

7.2.1 Principle of operation

The basic element of the GEM detector is a thin, self-supporting layered mesh realized by the conventional photo-lithographic methods used to produce multilayer printed circuits. A thin insulating polymer foil metallized on each side is passivated with photo-resist and exposed to light through a mask; after curing, the metal is patterned on both sides by wet etching and serves as self-alignment mask for the etching of the insulator in the open channels. Because of the etching process, holes are conical in shape from both entry sides, probably improving the dielectric rigidity. Thanks to the focusing effect of the field, one expects full efficiency for transfer of charge, and the dense channel spacing reduces image distortions. For the device to properly function, a good and regular insulation between the grid electrodes is required, with no sharp edges, metallic fragments or conducting deposits in the channel; this has been obtained by careful optimization of the etching and cleaning procedures.

For convenience, the MWPC is operated with the anode wires at positive potentials, the signals being picking up through HV decoupling capacitors; this choice allows to maintain the lower electrode of GEM at ground potential, and easily increase the multiplying voltage.

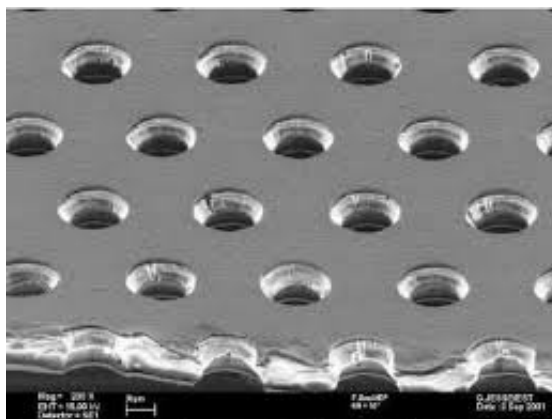


Figure 7.4: Image of the GEM foil taken with an electron microscope.

The standard CERN GEMs consist of an insulator made of a thin Kapton foil (about $50 \mu m$) which is coated on both sides with copper layers (about $5 \mu m$). This structure is perforated with holes that typically have a diameter of $70 \mu m$ and a pitch of $140 \mu m$. The holes are arranged in a hexagonal pattern. Due to an etching production process they have a double conical shape with an inner diameter of about $50 \mu m$. Besides the CERN GEMs, also other companies are now producing GEM foils, that vary in hole size, shape as well as the insulator thickness and material. Figure(7.4) shows a picture of a GEM that has been taken with an electron microscope. Here GEM means single GEM at all the considerations.

Most electric field lines end on the side towards the cathode while on the other side most lines go into the direction of the anode. The ions from the gas amplification are pulled to and collected on the GEM surface while most of the electrons are extracted out of the GEM holes. The electron extraction is intensified if additionally a magnetic field is applied perpendicular to the GEM plane. The electrons tend to follow the magnetic field lines. The intrinsic ion back-drift suppression is one of the main advantages of the GEMs and makes a gating grid unnecessary. Operation of wire chambers typically involved only one voltage setting: the voltage on the wire

provided both the drift field and the amplification field. A GEM-based detector requires several independent voltage settings: a drift voltage to guide electrons from the ionization point to the GEM, an amplification voltage, and an extraction/transfer voltage to guide electrons from the GEM exit to the readout plane. A detector with a large drift region can be operated as a time projection chamber; a detector with a smaller drift region operates as a simple proportional counter.

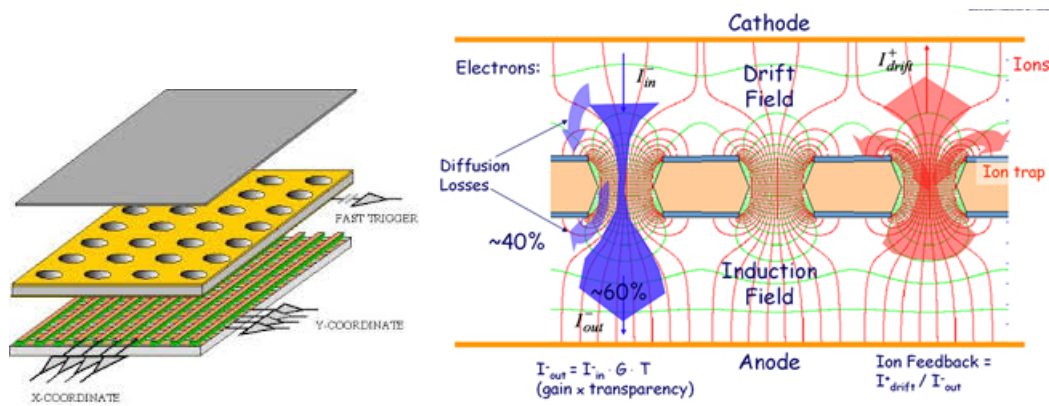


Figure 7.5: Schematic diagram of a GEM detector's readout.

A GEM chamber can be read-out by simple conductive strips laid across a flat plane; the readout plane, like the GEM itself, can be fabricated with ordinary lithography techniques on ordinary circuit board materials. Since the readout strips are not involved in the amplification process, they can be made in any shape; 2-D strips and grids, hexagonal pads, radial/azimuthal segments, and other readout geometries are possible. One notable early user was the COMPASS experiment at CERN. GEM-based gas detectors have been proposed for components of the International Linear Collider, the STAR experiment and PHENIX experiment at the Relativistic Heavy Ion Collider, and others. The advantages of GEMs, compared to multiwire proportional chambers, include: ease of manufacturing, since large-area GEMs can in principle be mass-produced, while wire chambers require labor-intensive and error-

prone assembly; flexible geometry, both for the GEM and the readout pads; and suppression of positive ions, which was a source of field distortions in time-projection chambers operated at high rates. A number of manufacturing difficulties plagued early GEMs, including non-uniformity and short circuits, but these have to a large extent been resolved.

For the GEM-TPC upgrade of ALICE, it is mandatory to minimize the ion backflow as a prerequisite for continuous readout and maintenance of excellent TPC performance. GEM foils as a charge amplifier are the candidate to operate a TPC in continuous readout mode. The GEM technology has been established in the last decade as a robust and well proved amplification technique for gaseous detectors with excellent results for spatial resolution, transverse and longitudinal hit separation and low ion backflow.

The model of a basic GEM cell built using Garfield, is shown in fig- 7.6. It represents a GEM foil, having two bi-conical shaped holes placed in a staggered manner along with a readout anode and a drift plane on either sides of the foil. The distance between top surface of the GEM and the drift plane is called the drift gap whereas that between the lower surface and the readout plate is named induction gap. With the help of this model, the field configuration of the detectors has been simulated using appropriate voltage settings. These are followed by the simulation of electron transmission and ion backflow fraction in Ne/CO₂/N₂ (90/10/5) gas mixture.

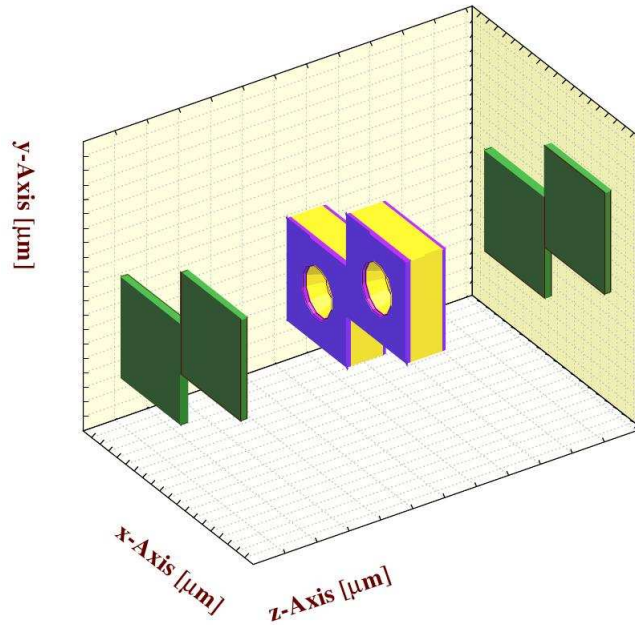


Figure 7.6: Basic GEM cell built using Garfield.

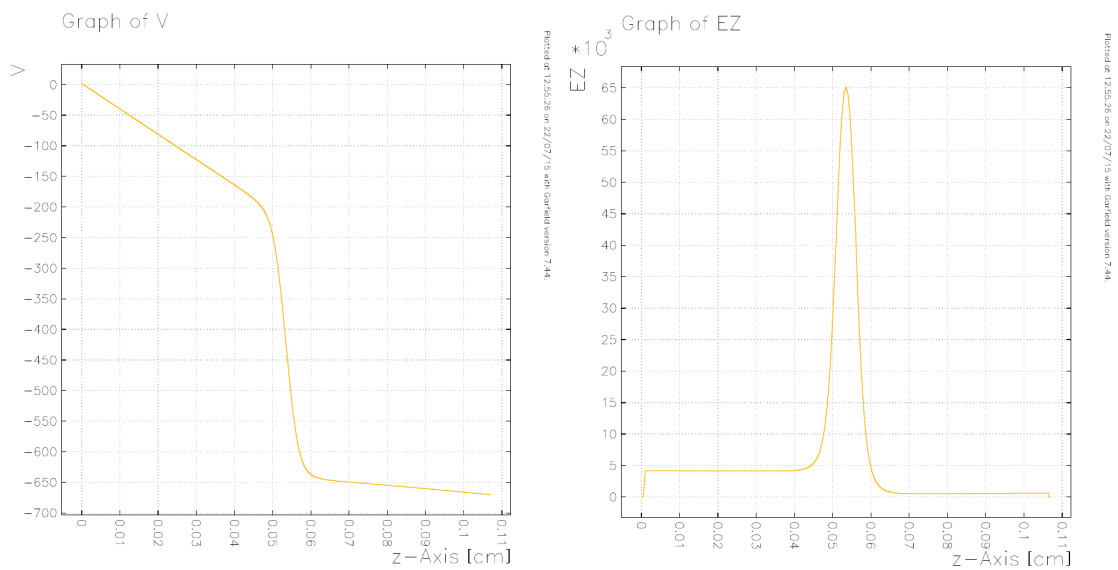


Figure 7.7: Voltage and Electric field along the z-axis passing through hole of a GEM.

Drift lines:- The electrons, without being affected by the diffusion, follow the field lines. Due to the high field gradient between the drift volume and the GEM hole, the field lines are compressed, resulting in a characteristic funnel shape. The decrease of E_{gem} for a particular E_{drift} or the increase of E_{drift} at a fixed E_{gem} , affects the funneling, resulting in the termination of the drift field line on the top cathode surface of the GEM foil.

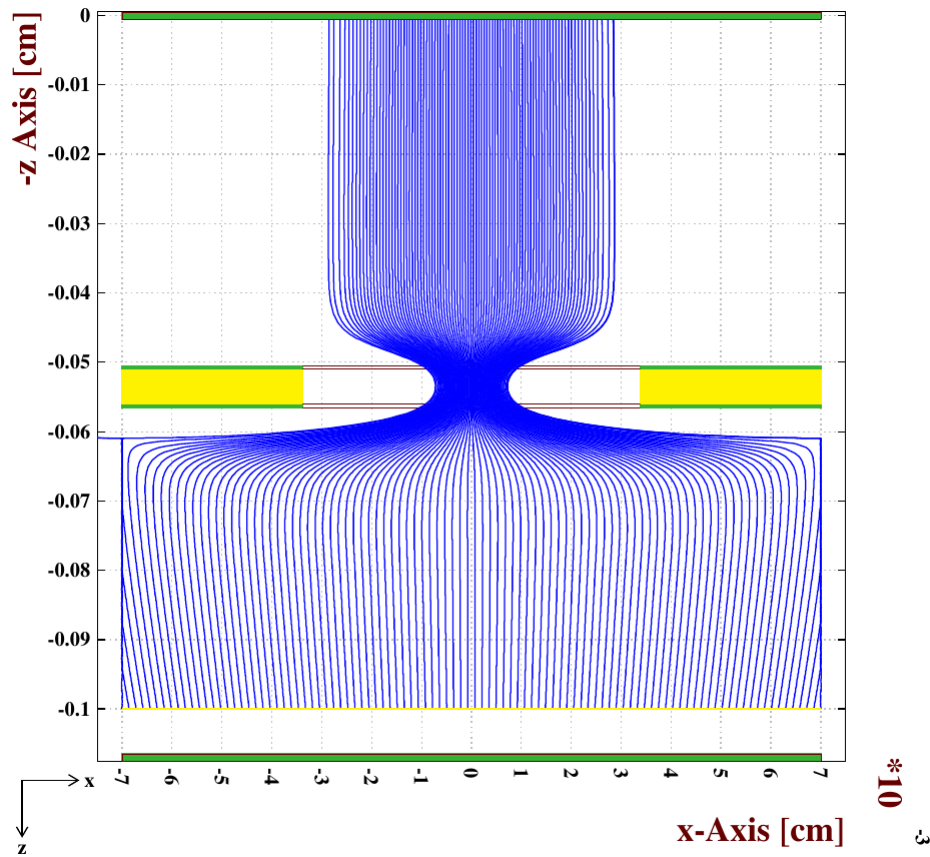


Figure 7.8: Electron drift lines in GEM.

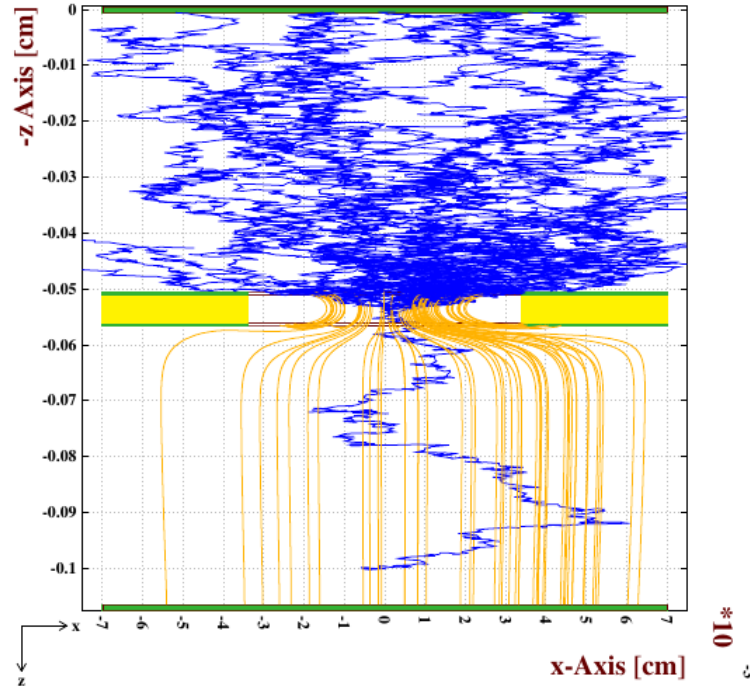


Figure 7.9: A simulated avalanche, drift and the diffusion of secondary electrons (blue) and ions (yellow).

7.2.2 Results

For the calculation of electron transmission, 10000 electrons have been injected in the drift gap in random position. These electrons are made to drift towards the GEM foil. The electron transmission has been estimated as the ratio between the number of electrons that reach the anode plate to the number of electrons created in the drift volume. For a single GEM detector, the total electron transmission (ϵ_{tot}) can be identified as the multiplication of two efficiencies, the collection efficiency (ϵ_{coll}) and the extraction efficiency (ϵ_{ext}).

$$\epsilon_{tot} = \epsilon_{coll} \times \epsilon_{ext} \quad (7.1)$$

The collection efficiency has been defined as:

$$\epsilon_{coll} = \frac{\text{Electrons reached inside the GEM foil}}{\text{Electrons created in drift volume}} \quad (7.2)$$

The extraction efficiency has been defined as:

$$\epsilon_{ext} = \frac{\text{Electrons reached the readout plane}}{\text{Electrons presented inside the GEM foil}} \quad (7.3)$$

The field geometry has a strong impact on ϵ_{coll} and ϵ_{ext} and thus on ϵ_{tot} . A decrease in the ratio E_{GEM}/E_{Drift} results in the termination of the drift lines on the top surface of the GEM foil leading to a loss of ϵ_{coll} . With a decreasing ratio $E_{Induction}/E_{GEM}$, more drift lines are attracted by the bottom surface of the GEM foil leading to a loss of ϵ_{ext} . Again, depending on these two field ratios, some drift lines also end at the dielectric substrate. In reality, the electron trajectories are affected by the diffusion and the loss of electrons on different electrodes increases due to diffusion which naturally affects ϵ_{coll} and ϵ_{ext} . Besides that, the electron attachment coefficient, can also influence transmission. The variations of ϵ_{coll} , ϵ_{ext} and ϵ_{tot} under different field configurations have been plotted in following figures.

For a fixed V_{GEM} and $E_{Induction}$, ϵ_{coll} and thus ϵ_{tot} , decrease with the increase of the drift field, whereas no significant effects of drift field on ϵ_{ext} has been observed (figure). Similarly, at a fixed V_{GEM} and E_{Drift} , the increase of induction field, increases ϵ_{ext} as shown in fig 7.11. The change of V_{GEM} only has effect on ϵ_{coll} and thus ϵ_{tot} (figure). It is also seen from fig 7.12, for the same voltage configuration, the smaller pitch GEM foils is better in terms of higher electron transmission, whereas no significant effect of 0.5 T magnetic field has been observed.

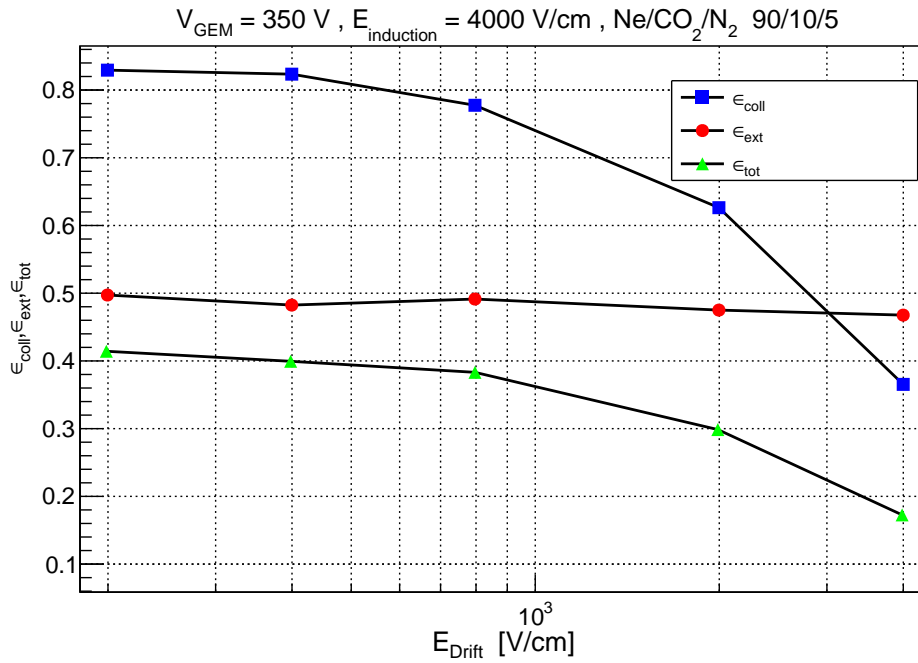


Figure 7.10: Variation of electron transmission and efficiencies as a function of drift field.

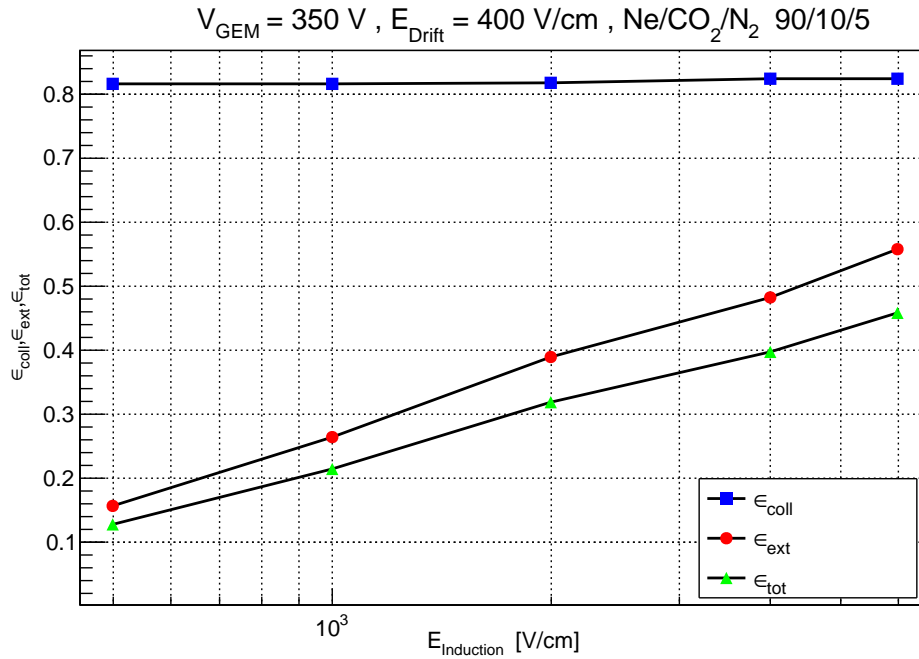


Figure 7.11: Variation of electron transmission and efficiencies as a function of induction field.

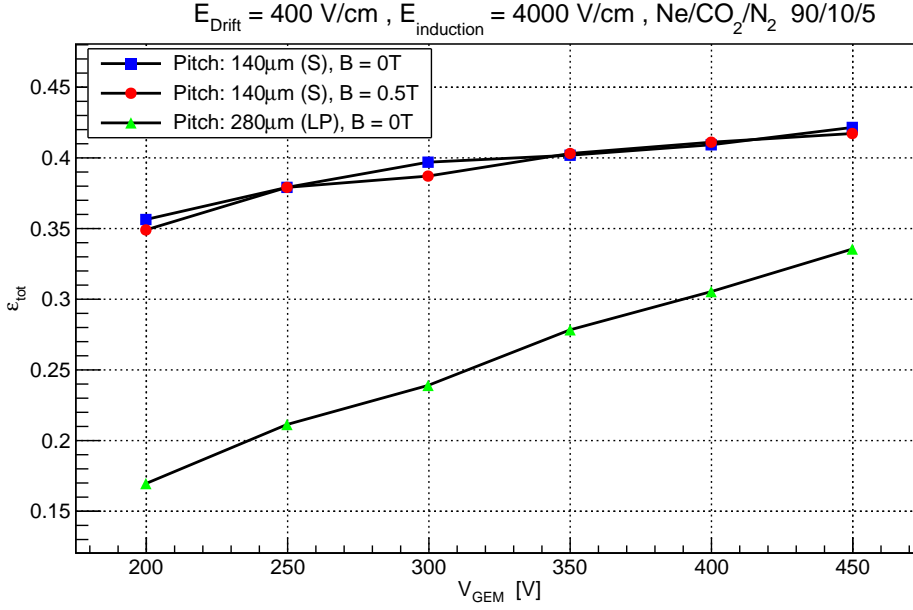


Figure 7.12: Variation of electron transmission and efficiencies a function of GEM voltage (For different pitch).

The electrons during their drift produce avalanche inside the GEM foil. The primary ions in the drift region and the ions created in the avalanche have been considered for the estimation. The backflow fraction has been calculated as

$$IBF = \frac{N_{id}}{N_{iT}} \quad (7.4)$$

where N_{id} is the number of ions collected at the drift plane and N_{iT} is the number of total ions. As mentioned earlier, the ions drifting back to the drift volume, can disturb the homogeneity of the drift field and, thus, distort the behaviour of the detector. In order to prevent those ions from entering the drift volume, a proper optimization of the field in the drift volume, GEM hole and induction regions is necessary (figure 7.13).

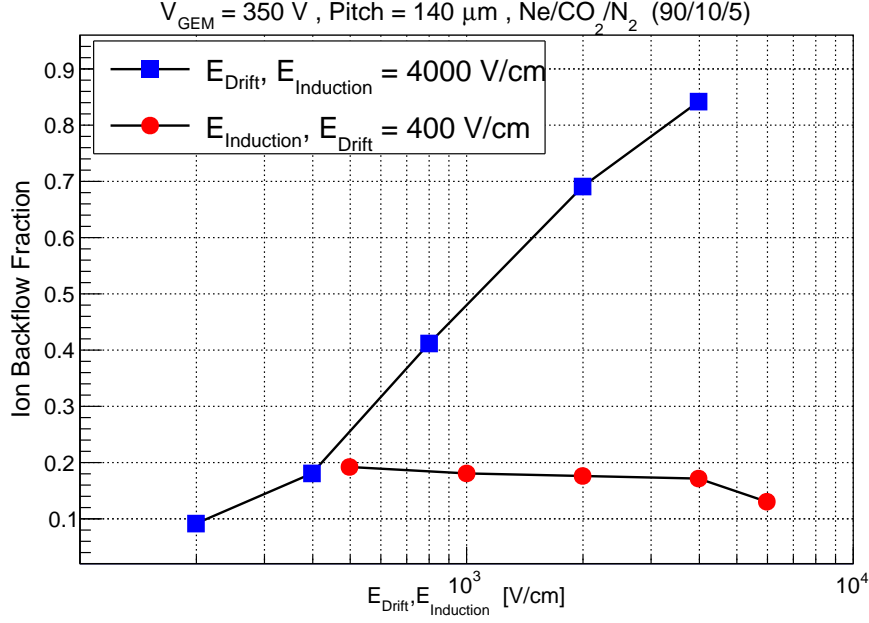


Figure 7.13: Variation of IBF a function of drift and induction field.

The ion backflow of a single GEM can be reduced by decreasing E_{Drift} because less number of field lines will get out of the hole into the drift volume. At higher E_{Drift} , the ratio between and E_{GEM} is large resulting in the drift of more number of ions into the drift volumm. At higher E_{GEM} , the ratio between E_{Drift} and E_{GEM} is small and thus a large fraction of ions is collected at the top surface of the GEM foil. No significant effect of $E_{\text{Induction}}$ has been observed except at the higher $E_{\text{Induction}}$. From the figure 7.14, it is also seen that the GEM foil with smaller pitch is better in terms of lower backflow fraction, whereas no significant effect of 0.5T magnetic field on backflow has been observed.

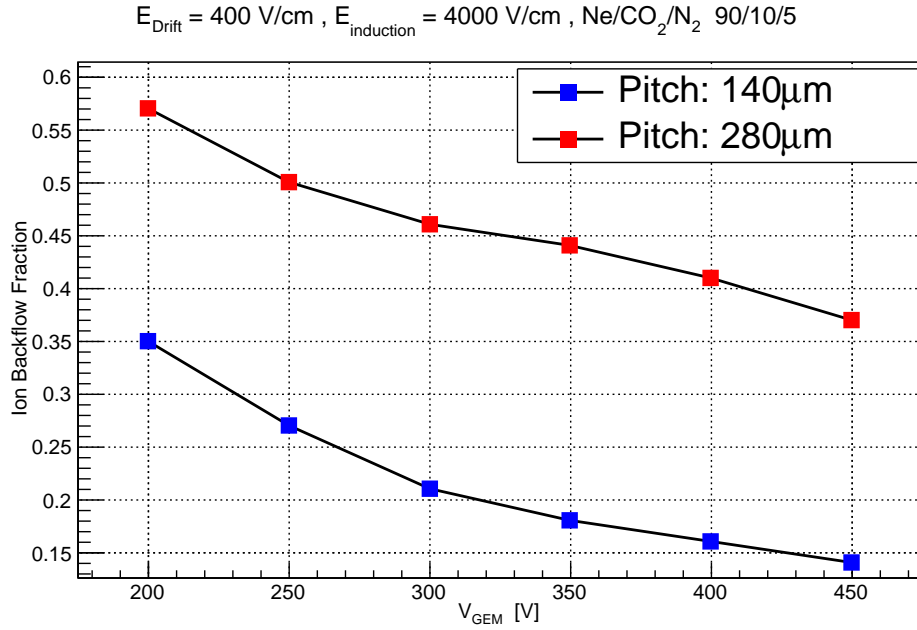


Figure 7.14: Variation of IBF as a function of GEM voltage (For different pitch).

The Avalanche routine of Garfield software has been used. The procedure first drifts an initial electron from the specified starting point. At each step, a number of secondary electrons is produced according to the local Townsend and attachment coefficients and the newly produced electrons are traced like the initial electrons.

Changing the three voltage differences the variation of GEM gain is checked. Gain is plotted below with varying GEM voltage in a log scale. Then it has been fitted with an exponential function.

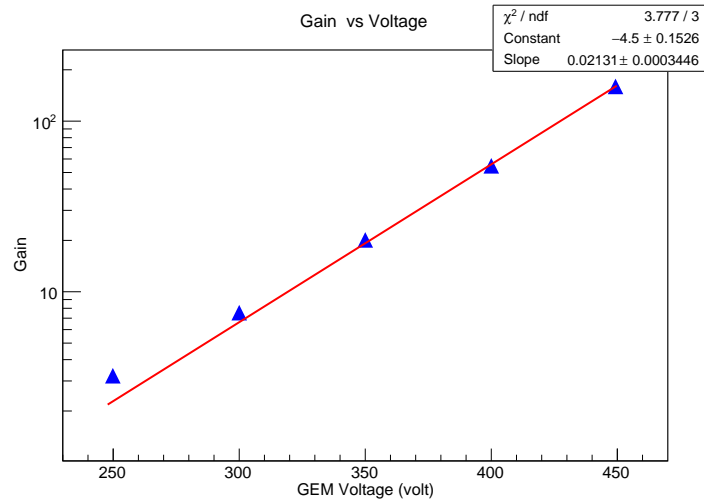


Figure 7.15: Variation of Gain as a function of GEM Voltage.

Which shows that the avalanche process amplifies more with increasing electric field between the GEM plates.

7.2.3 Conclusion

As the increment in voltage across the GEM foil increases the gain, electron transmission and decreases the IBF, high GEM voltage should be preferred. Lower pitch ($140\mu m$) and low drift field allows low IBF values and high electron transmission. Induction field should be high as it increases the electron transmission.

Chapter 8

Summary and Conclusions

We have discussed the principles of the operation of the gaseous detectors focusing on the most relevant mechanisms involved in the detection process. This knowledge is necessary to understand and optimize the performance of a proposed or any existing detection systems. In our work we have used the Garfield simulation framework for carrying out the simulation of the physical processes in different MPGDs. This framework was augmented in 2009 through the addition of the neBEM toolkit to carry out 3D electrostatic field simulation. Besides neBEM, the Garfield framework provides interfaces to Magboltz for computing the transport and amplification property. We have discussed about these simulation tools. To understand the software in details, we have also presented some useful results using these tools as stand-alone routines. Starting with the discussion of an MWPC, we have emphasized our focus on the MPGDs. Among several MPGDs, we have given a somewhat detailed description, advantages and disadvantages of GEM detector. In the present work, numerical simulation has been used as a tool of exploration to evaluate the fundamental features of a single GEM detector. The study includes extensive computation of electrostatic field configuration within a given device. Some of the fundamental properties like gain, electron transmission, ion backflow and their dependence on different voltage configurations, have been estimated too.

References

- [1] W. Blum and L. Rolandi, Particle detection with drift chambers
- [2] Glenn F. Knoll, Radiation Detection and Measurement
- [3] W. R. Leo, Techniques for Nuclear and Particle Physics Experiments
- [4] K. Kleinknecht, Detectors for particle radiation; Cambridge Press, Cambridge, 2 nd Edition (1998).
- [5] S. Mukhopadhyay et al., neBEM: a Field Solver; RD51 Internal Note-2009-001.
- [6] S.F. Biagi; Monte Carlo simulation of electron drift and diffusion in counting gases under the influence of electric and magnetic field; Nucl. Instrum. Meth. A vol. 421 (1999) 234.
- [7] T. Aoyama, Genneralized Gas Gain Formula For Proportional Counters, Nuclear Instruments and Methods in Physics Research A 234 (1985) 125-131
- [8] G. Charpak et al., Multiwire proportional chambers and drift chambers; Nucl. Instrum. Meth. vol. 162 (1979) 405.
- [9] S.Biagi; Magboltz-Transport of electrons in gas mixture; <http://cern.ch/magboltz>. and for the cross sections "http://rjd.web.cern.ch/rjd/cgi-bin/cross"
- [10] S.D.Pinto-'GAS ELECTRON MULTIPLIERS VERSUS MULTIWIRED PROPORTIONAL CHAMBERS' (arXiv:1309.2908v1 [physics.ins-det] 11 Sep 2013)
- [11] F. Sauli, GEM: A new concept for electron amplification in gas detectors; Nucl. Instrum. Meth. A vol. 386 (1997) 531.

- [12] <http://garfield.web.cern.ch/garfield/>
- [13] <http://magboltz.web.cern.ch/magboltz/>
- [14] Asoskov V.S., Chechin V.A., Grichine V.M. at el, Lebedev Institute annual report, v. 140, p. 3 (1982)
- [15] Fano U., and Cooper J.W. Rev.Mod.Phys., v. 40, p. 441 (1968)
- [16] Biggs F., and Lighthill R., Preprint Sandia Laboratory, SAND 87-0070 (1990)
- [17] Allison W.W.M., and Cobb J. Ann.Rev.Nucl.Part.Sci., v.30,p.253 (1980)
- [18] John David Jackson Classical Electrodynamics John Wiley Sons Ltd. 1962
- [19] SIMON RAMO - Current Induced by Electron Motion